1-1-2005

Investigation into the onset of nanoscale surface damage of biomedical grade CoCrMo: influence of contact loads, residual stresses, and environment

Andrew Scott Mitchell
Iowa State University

Investigation into the onset of nanoscale surface damage of biomedical grade CoCrMo: Influence of contact loads, residual stresses, and environment

by

Andrew Scott Mitchell

A thesis submitted to the graduate faculty

in partial fulfillment of the requirements for the degree of

MASTER OF SCIENCE

Major: Mechanical Engineering

Program of Study Committee:
Pranav Shrotriya, Major Professor
Sriram Sundararajan
Brian Gleeson
Michael Conzemius

Iowa State University
Ames, IA
2005

Graduate College
Iowa State University

This is to certify that the master's thesis of

Andrew Scott Mitchell

has met the thesis requirements of Iowa State University

Signatures have been redacted for privacy

Table of Contents

Chapter 1. General Introduction

1.1 Bearing Surfaces in Total Hip Replacements

Total joint replacements are mechanical devices used to replace worn out or damaged human joints. The total hip replacement (THR) is composed of three distinct components: femoral stem, femoral head, and acetabular cup (figure1). The femoral stem is implanted into the patient's femur, the femoral head is then connected to the stem by interlocking tapers (Morse tapers). This modular design has become popular since it allows orthopedic surgeons a great deal of latitude in customization while maintaining a small inventory of components.

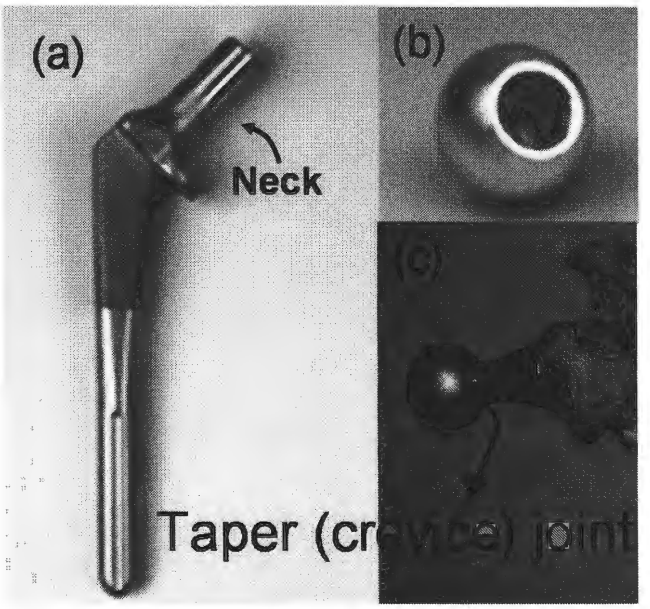

Figure 1 A) The femoral stem of a hip prosthesis. B) The femoral head. C) This figure depicts the crevice geometry formed when the femoral head and stem are connected.

Titanium alloys (Ti-6Al-4V, ASTM F-136) or Cobalt alloys (CoCrMo, ASTM F75 cast and ASTM 562, ASTM F799, ASTM F1537 wrought) generally make up the femoral stem while the femoral head may be composed of the former metals, ceramic alumina (Al_2O_3 ASTM F603), or ceramic zirconia (ZrO2 ASTM F1873) [1, 2]. The acetabular cup may be composed of the latter materials or an ultra high molecular weight polyethylene. The primary bearing surfaces in a total hip replacement are between the acetabular cup and the head as well as the femoral head and the stem. The area of interest in the present

investigation is between the head and the stem where the interlocking tapers have a tendency to be subjected to phenomena termed fretting corrosion, to be discussed later. Wear debris caused from these contacts has been cited as the cause for such trouble as osteolysis (degradation of bone tissue), aseptic loosening, failure of the implant, and inflammation often leading to revision surgeries [1, 3].

A National Hospital Discharge Survey (2003) [4] indicated that nearly 150,000 patients in the United States received total hip replacements in 2003. In addition 30,000 revisions of previous surgeries were preformed in 2003. The American Academy of Orthopaedic Surgeons has projected the number of initial surgeries to double by the year 2030. A study preformed by the Canadian Institute for Health Information [5] revealed that 10% of all hip surgeries in a given year were revisions of previous surgeries. The three major causes of revision surgery were determined to be loosening (61%), osteolysis (34%), and wear (29%). As indicated by the statistics these issues are not mutually exclusive. Wear debris may lead to osteolysis both of which may contribute to loosening of the implant. The need to extend biomedical implant life is prevalent considering an increased aging population with longer life expectancies. As alluded to earlier, fretting corrosion is a serious problem that limits the useful life of implants through the generation of wear debris and mechanical failure.

1.2 Fretting Corrosion

Fretting wear occurs when two bodies in contact experience small relative oscillations of the order of tens of micrometers to hundreds of micrometers (microns). Fretting Corrosion is the combination of fretting wear and a corrosive environment. Fretting is noted in applications such as the dovetail joint of turbine blades, biomedical implant joints, cables, and between nuclear fuel rods and spacers to name a few. Fretting wear/corrosion accelerates the crack initiation process, reducing the overall fatigue life of components. This may lead to in-service failures or costly preventative maintenance. In the case of biomedical joints preventive maintenance is essentially impossible, leaving only the option of ultimate failure by wear of the implant or physiological reactions to the wear debris. It is obvious then that a comprehensive model of fretting is essential from a design perspective. However,

a complete phenomenological equation for fretting wear/corrosion remains elusive do to its complex synergistic nature. Factors that affect the fretting rate of materials include: the amplitude of the cyclic slip displacement; mismatch of elastic/plastic properties of the contacting surfaces; coefficient of friction; asperity roughness; environment; residual stresses; mechanical loads; and phase transformations produced by local temperature variations [6].

1.3 Brief Literature Review

Gilbert et al. examined one hundred and forty eight retrieved modular hip prostheses and found a significant amount of corrosion at the head/neck interface [7]. In this study the researchers hypothesize the damage mechanism proceeds by local delamination of the oxide film covering the metal followed by rapid repassivation. The modular design of the femoral head/neck creates a crevice where physiological fluid may become trapped. The delamination/repassivation of the film consumes oxygen in the crevice which ultimately leads to differential aeration and local drops in the pH. This process will continue until the oxide film becomes unstable due to the acidic environment and can no longer repassivate. At this point the metallic substrate would undergo active corrosion. Brown et al. supported this theory by demonstrating that the modular joint will not be subjected to crevice attack in the absence of loading [8]. In addition, the researchers demonstrate that mixed alloy couples (Ti-alloys on Co-alloys) do not promote galvanic attacks. Brown et al. also performed cyclic tests on the femoral stem/head coupling by loading the prostheses in a universal testing machine while in a saline bath. The objective was to determine the optimal design for the length of neck extension on the femoral stem. The tests revealed that longer neck extension were more prone to fretting than the shorter extensions. This is indicative of the applied load affecting the fretting corrosion. Hallab et al. [2] uses a similar approach to Brown et al. however the femoral stem/head are monitored for wear debris release by placing a potentiostat in the bath. The current in the system is then monitored, showing increases when debris is released into the system. It was revealed that ceramic heads on metal stems actually released less debris and performed better overall than metal-metal couples. Several other groups have attempted to examine the wear debris generation as well. These studies

utilize more sophisticated commercially available hip simulators [9, 10]. Whereas the universal testing machines used by Brown et al. [8, 11] and Hallab et al. [2]are only capable of applying a single loading condition (normal); commercial available hip simulators are capable of applying several different loading conditions simultaneously including normal, torsional, and flexural.

Catelas et al. [10] and Fisher et al. [9] each examined wear particles of metal on metal (specifically CoCr-CoCr) contact between the acetabular cup and the femoral head using commercially available hip simulators. While this is not the surface undergoing fretting corrosion the results of the studies are quite interesting and provide insight into the fretting dilemma. Each study demonstrated a run in period which occurred at under one half million cycles at which point the alloy reaches a steady state wear condition. Catelas et al. retrieved wear particles throughout long term testing of the implant and found primarily Chrome oxide debris, indicating that it is the dominant oxide covering the alloy. Also, it may be concluded that chrome oxide dominates the repassivated film as well since throughout the 3 million cycle test chrome oxide debris were predominant. This study compared three different alloys of CoCr: as cast, low carbon wrought, and a high carbon wrought. The high carbon wrought alloy exhibited the least damage and wear followed closely by the cast alloy. The low carbon alloy was significantly less impressive at inhibiting wear. While some of the performance may be attributed to the microstructure the residual stress in the material should not be overlooked. Just by the nature of the alloying the cast alloy should contain very little pre-stress while the wrought alloy would be expected to have a significant amount.

While previous research has examined the role of material pairing, microstructure, mechanical loading, and environment on fretting there is a disproportionate amount of research on the effects of residual stress in biomedical applications. In fact to the authors knowledge there has been no studies conducted to date to examine residual stress effects on fretting in biomedical prostheses. Residual stress will manifests itself through repeated asperity level loadings during fretting, through the manufacturing process, or through surface treatments such as shot peening.

Surface treatments are widely used in industry to induce compressive residual stresses. Research has demonstrated that compressive residual stresses are generally

beneficial at mitigating surface damage[9, 12, 13]. Treatments such as nitriding or thin surface coatings often display excellent wear resistance and are considered as inducing compressive residual stress [9, 13]. While compressive stresses are induced the magnitude is such that the interfacial hardness may increase up to six times its original value, which in turn mitigates surface damage. This is analogous to changing the material pairing; consequently treatments such as these do not provide a good understanding of the role of residual stress. Shot peening on the other hand affords insight into the role residual stress, since the change in interfacial hardness is not as drastic.

Bonner et al. [14] has demonstrated that shot peened stainless steel specimens will undergo a stress relaxation with material removal. Benrabah et al. [15] also demonstrates this when studying fretting of shot peened samples. Interestingly, Benrabah et al. discovered that the maximum stress relaxation occurs within the first 300 cycles of testing. In addition, it was found that wear debris generated within the initial stages of fretting acted as a solid lubricant inhibiting the wear. The notion of beneficial three body wear is not a novel concept. Earlier work by Iwabuchi [16] noted that oxide particles will either inhibit wear by lubricating the surface or accelerate wear as traditionally thought depending on the nature of the slip amplitude and normal loading. These concepts will be discussed in more depth in chapter 3.

1.4 Research Objectives

The importance of understanding every aspect of fretting is crucial in determining a proper design philosophy. At the current time there is a lack of a mechanistic understanding regarding the role of surface residual stresses in fretting. Moreover, there is an absence of information regarding the behavior of residual stressed material undergoing fretting in different oxidative environments. Research on the nature of residually stressed materials in fretting scenarios has been limited to shot peened specimens where the surface stress state must be determined by x-ray diffraction. These tests incorporate a spherical or rectangular contact pad, which produces nominal contact areas on the order of millimeters. The limited capabilities of this approach have instigated the development of a novel experimental setup to investigate a range of residual stresses while applying contact loads over a predetermined

real area of contact. This study incorporates a four-point bending frame in conjunction with an atomic force microscope (AFM). The intention is to develop a basic mechanistic understanding of the failure process taking place during fretting. The setup described throughout this work is only meant as a means of gaining understanding of the local failure of the oxide film and is limited in that it cannot provide long term wear performance data. It is hoped that the results provided will ultimately contribute to an encompassing phenomenological fretting model that may be used when designing with materials that form a passive film.

1.5 Thesis Outline

The thesis consists of a brief chapter illustrating the design of the four point bending frame followed by two chapters, each composed of a paper to be submitted for publication. The papers follow a typical format consisting of an abstract, introduction, experimental methods, results and discussions, and a conclusion.

In Chapter 3 the fretting wear of CoCrMo will be investigated in ambient conditions using the frame discussed in Chapter 2 and the atomic force microscope (AFM). The chapter will focus largely on the experimental technique developed and the results of the wear in an ambient environment. Details of the experimental technique will include discussions on the possible sources of error in this experimental technique. In addition, a damage mechanism based on the amount of energy dissipation allowed in the substrate is hypothesized.

Chapter 4 will describe the results achieved in an aqueous environment. The results will be briefly compared with the ambient condition reemphasizing the hypothesized damage mechanism proposed in chapter 3. The damage mechanism will then be extrapolated to include caustic environments. The nature of the residual stress in the dissolution/repassivation process will be discussed in terms of previous research.

Chapter 2. Design of a Loading Frame: Considerations and Approach

2.1 Design Considerations

A frame was designed to apply known levels of stress to a sample. The design philosophy was that the stress state could be determined independent of the sample's material properties. Additionally, the frame would have to be adjustable to accommodate different geometries of samples and apply stress levels below the yield point of the sample. The overall design constraint for the frame was the dimension between the AFM scanner and stage. This allows for a height of less then three quarters of an inch to place the frame. The frame applies stress to a sample while the AFM scratches the exposed face of the sample. The applied normal loading as well as the surface residual stress produced by the frame may be studied simultaneously to determine their roles in the surface damage mechanism. In the following section the design and theory behind the loading frame will be discussed.

It was determined that a similar design [17] employed for the purpose of monitoring surface roughness evolution fit these requirements. This design incorporates a clamp like structure (c-clamp) that fits over a base with an extrusion (base) (figures 2a, 2b).

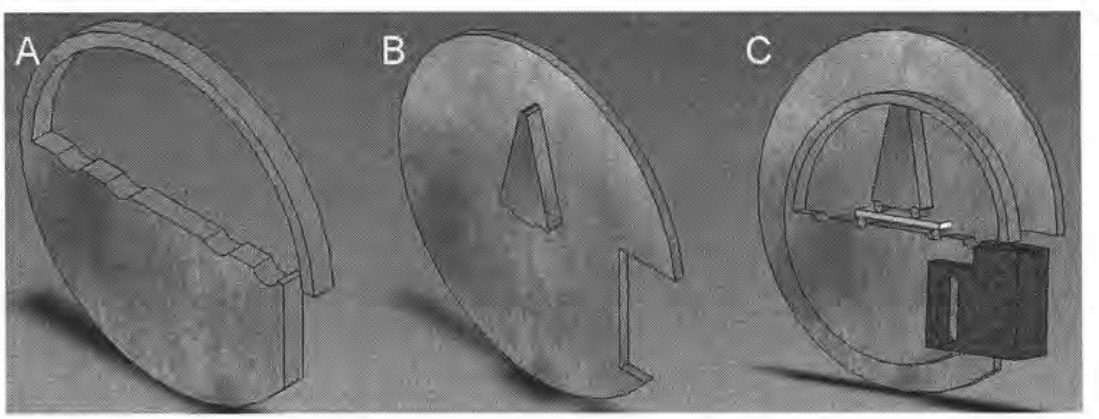

Figure 2 A) Image of the c-clamp B) Base with extrusion C) Depiction of the entire assembly when the rollers and sample are added. The darker casing on the right hand side is the holder protecting the capacitance gage.

As the rollers and rectangular sample are inserted in between the c-clamp and the extrusion on the base, a force (P) is exerted onto the c-clamp causing it to open (figure 3).

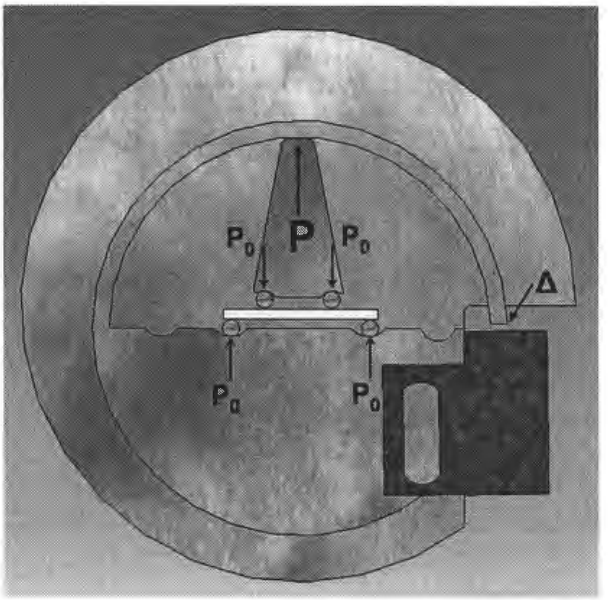

Figure 3 The rollers and sample are placed in-between the base and c-clamp causing a force to be exerted from the base onto the c-clamp (P). P_0 depicts the load transmitted to the rollers while Δ is the measured free end deflection of the clamp.

This force would then be distributed across the four rollers at half of the magnitude (P_0=P/2). In order to determine the force (P) it is necessary to monitor the change in the free end deflection of the c-clamp (Δ). The change in the free end deflection is obtained by a capacitance gage attached to the c-clamp. The capacitance gage measures the air gap between the sensor and end of the c-clamp by monitoring the capacitive reactance. Hence, it acts like a parallel plate capacitor in an AC circuit. The non-contact nature of the capacitance gage coupled to a fine resolution (hundreds of nanometers) provides an ideal tool for measuring the deflection of the beam.

The selection of the gage was based off of several criteria: non contact sensor, ease of use, and secondary safety device for the design. The most important being a non-contact sensor so that the deflection of the clamp would be unhindered. This narrows the possibility to either optical means (laser / fiber optics) or electrical systems (capacitance / inductance). The simplest to implement is the capacitance gage since it requires only fixing components to the base and not to the arm itself. In addition, the capacitance gage is relatively small (mm in diameter) and can be removed easily once the measurement is preformed. The specific gage

chosen for this task was the Capacitec HBP-75, with a linear range of a little over 1mm. The third main criterion is that the gage would provide a secondary check to not exceed the limits of the c-clamp. A factor of safety of two on the design of the c-clamp permits the end deflection to be at 1mm, in agreement with the range of the capacitance gage. If the clamp is loaded beyond the factor of safety the gage will shut off warning the user of the overload on the c-clamp's arm.

To accommodate samples of varying thickness and stiffness rollers of different diameter may be employed. The rollers need to be hard enough not to deform when placed in the clamp. Pin gages (Go/No Go gages) of various diameters were cut to a desired length and used as rollers. These gages are heat treated 52100 bearing steel and lapped to a precise finish (+or-10 μm). It was found that this material is very acceptable to sustain the maximum force experience by the rollers, around 2.5 lbs.

2.2 Calibration

To accurately account for the amount of load experienced by the clamp, the clamp was calibrated by a dead weight method. Calibration weights were suspended from the apex of the c-clamp's arm in increments of 0.1 lbs until a max of 4 lbs was reached. At each increment the deflection of the clamp was recorded using the reading from the capacitance gage. This calibration was preformed over five independent trials. The calibration chart (figure 4) displays the average deflection readings across the five trials for each load. The error bars are plus and minus one standard deviation but are not much larger than the symbols. A linear regression of the data displays the relationship between the free end deflection of the clamp (δ) and the force applied (P) at the apex of the c-clamp's arm. This relationship is used to calculate the amount of applied load on the sample.

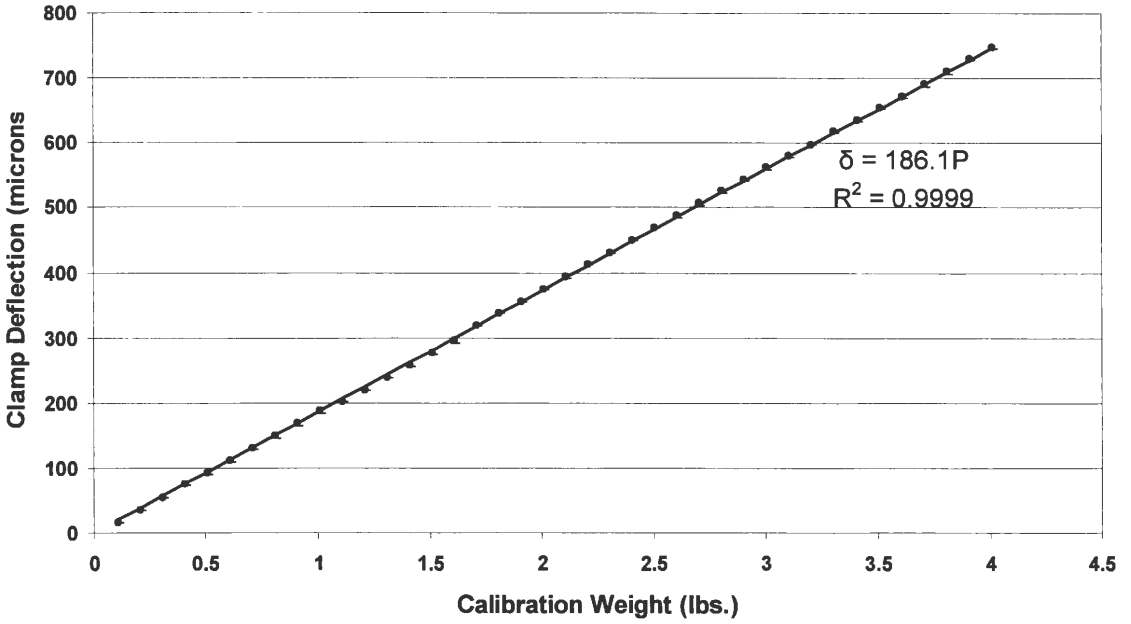

Figure 4 Calibration chart demonstrating the relationship between the applied loading and the free end deflection of the clamp.

2.3 Theory of Operation

As mentioned previously it is ideal to be able to measure the stress in the sample without knowing material properties. The nature of this setup allows for just this. Consider a sample loaded in four point bending (figure 5). From the shear force and moment diagram (figure 5) it is apparent that a constant moment is developed between the two inner most rollers. Using the stress equation for rectangular beams in bending:

$$\sigma = \frac{Mc}{I} \qquad (1)$$

Where M is the constant moment, I is the second moment of area, and c is the distance from the neutral axis.

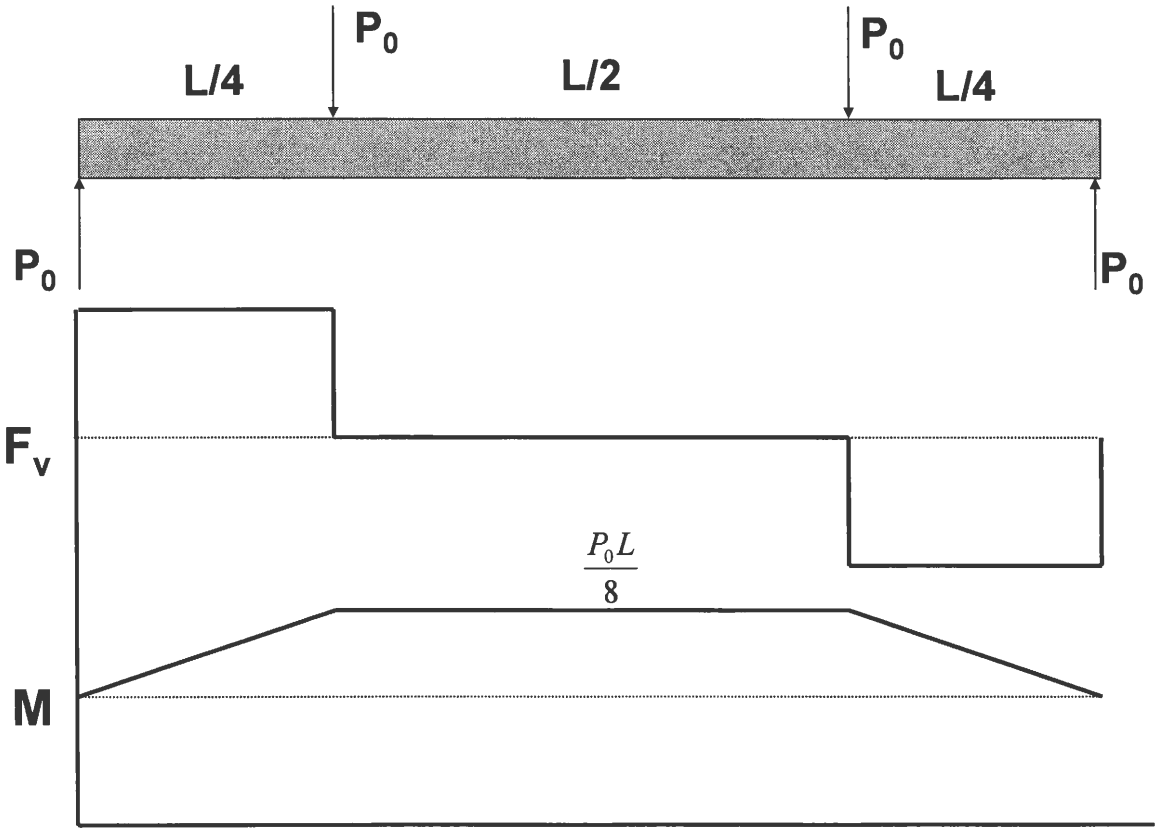

Figure 5 Shear force and moment diagram of a rectangular beam in four-point bending. Note that a constant moment is developed in-between the two center most rollers.

It is apparent that the stress state along the face of the beam will only be dependent on the geometry of the sample and the distance away from the neutral axis (center of the beam). Moreover, note that M and I are constant so the stress will vary only by the distance from the center of the neutral axis. This means that a single sample can provide a range of stresses from tensile to compressive across the face of the beam.

Once the sample is loaded and the deflection recorded, the moment (M) and second moment of area (I) are known. It is now vital to be able to calculate accurate distances from the neutral axis (c), so the stress state is known where the test is to be preformed. For this purpose a high resolution CCD camera is employed. The CCD camera is able to capture polishing pits and scratches. Using these defects as markers the number of pixels may be counted between the defects and the edge of the sample. This may be converted into a numerical distance by comparing the pixel ratio at different resolutions with a known

distance; in the current study a stage micrometer is used as the calibration sample. Prior to each experiment the sample is optically mapped to determine certain sites where tests may be conducted. When the loaded sample is placed beneath the AFM the defects may be located with the AFM camera so that scanning may take place along the same line of residual stress.

2.4 References

[1] N. J. Hallab and J. J. Jacobs, "Orthopedic implant fretting corrosion," *Corrosion Reviews*, vol. 21, pp. 183-213, 2003.

[2] N. J. Hallab, C. Messina, A. Skipor, and J. J. Jacobs, "Differences in the fretting corrosion of metal-metal and ceramic-metal modular junctions of total hip replacements," *Journal of Orthopaedic Research*, vol. 22, pp. 250-259, 2004.

[3] C. N. Kraft, B. Burian, O. Diedrich, and M. A. Wimmer, "Implications of orthopedic fretting corrosion particles on skeletal muscle microcirculation," *Journal of Materials Science: Materials in Medicine*, vol. 12, pp. 1057-1062, 2001.

[4] "Number of Patients, Number of Procedures, Average Patient Age, Average Length of Stay - National Hospital Discharge Survey 1999-2003," American Academy of Orthopaedic Surgeons.

[5] "More than 10% of Total Hip Replacements are for Repeat Surgeries, Reports Canadian Institute for Health Information (CIHI)," Canadian Institute for Health Information.

[6] S. Suresh, *Fatigue of Materials*, Second ed. New York: Cambridge University Press, 2003.

[7] J. L. Gilbert, C. A. Buckley, and J. J. Jacobs, "In vivo corrosion of modular hip prosthesis components in mixed and similar metal combinations. The effect of crevice, stress, motion, and alloy coupling," *Journal of Biomedical Materials Research*, vol. 27, pp. 1533-1544, 1993.

[8] S. A. Brown, C. A. C. Flemming, J. S. Kawalec, H. E. Placko, and C. Vassaux, "Fretting Corrosion Accelerates crevice corrosion of modular hip tapers," *Journal of Applied Biomaterials* vol. 6, pp. 19-26, 1995.

[9] J. Fisher, X. Q. Hu, T. D. Stewart, S. Williams, J. L. Tipper, E. Ingham, M. H. Stone, C. Davies, P. Hatto, J. Bolton, M. Riley, C. Hardaker, G. H. Isaac, and G. Berry, "Wear of surface engineered metal-on-metal hip prostheses," *Journal of Materials Science-Materials in Medicine*, vol. 15, pp. 225-235, 2004.

[10] I. Catelas, J. D. Bobyn, J. B. Medley, J. J. Krygier, D. J. Zukor, and O. L. Huk, "Size, shape, and composition of wear particles from metal-metal hip simulator testing: Effects of alloy and number of loading cycles," 2003.

[11] S. A. Brown, P. J. Hughes, and K. Merritt, "Invitro Studies of Fretting Corrosion of Orthopedic Materials," *Journal of Orthopaedic Research*, vol. 6, pp. 572-579, 1988.

[12] W. Ren, S. Mall, J. H. Sanders, and S. K. Sharma, "Evaluation of coatings on Ti-6Al-4V substrate under fretting fatigue," *Surface and Coatings Technology*, 2004.

[13] J. A. Hendry and R. M. Pilliar, "The fretting corrosion resistance of PVD surface-modified orthopedic implant alloys," *Journal of Biomedical Materials Research Part B: Applied Biomaterials*, vol. 58, pp. 156-166, 2001.

[14] N. W. Bonner, R. C. Wimpory, G. A. Webster, A. T. Fry, and F. A. Kandil, "Measurement of residual stress through a spot peened surface subjected to succesive material removal," *Materials Science Forum*, vol. 404-407, pp. 653-658, 2002.

[15] A. Benrabah, C. Langlade, and A. B. Vannes, "Residual Stresses and fretting fatigue," *Wear*, vol. 224, pp. 267-273, 1999.

[16] A. Iwabuchi, "The Role of Oxide Particles in the Fretting Wear of Mild-Steel," *Wear*, vol. 151, pp. 301-311, 1991.

[17] B. C. Burke, P. Shrotriya, and K. S. Kim: Brown University, 2003.

Chapter 3. Onset of nanoscale wear of metallic implant materials: Influence of surface residual stresses

A paper to be submitted to Scripta Materialia

Andrew Mitchell, Pranav Shrotriya
Department of Mechanical Engineering, Iowa State University, Ames, Iowa 50011, USA

3.1 Abstract

Nanoscale wear response of Cobalt-Chromium alloy (ASTM F-75) was investigated as a function of contact load and surface residual stress in order to identify mechanism governing onset of surface damage in modular implants. A unique loading configuration was utilized to apply range of known stress levels to the specimen surface. Using the tip of a scanning force microscope as a well characterized "asperity," controlled contact forces were applied on the specimen to mechanically stimulate the loaded surface. Volume of material removed was measured to characterize the wear rate as a function of the contact loads and surface stress state. Experimental measurements of nanoscale wear rate indicate that a critical level of contact pressure is required to initiate wear of the cobalt-chromium surface and as expected higher contact pressures accelerate the wear process. For a constant contact pressure, wear rate is accelerated by compressive residual surface stress while tensile residual stresses tend to suppress the surface wear. A surface damage mechanism based on successive delamination of native oxide layer due to single asperity contact and repassivation of exposed surface is proposed to elucidate the experimental observations.

Keywords: CoCrMo, Biomaterial, Wear, AFM, Fretting, Residual Stress

* corresponding author: Tel: +1 515-294-9719; email: shrotriy@iastate.edu

3.2 Introduction

Fretting contact between surfaces of artificial joints results in formation of particulate and soluble metallic debris that can migrate locally or systemically and may induce a cascade of inflammatory events that may ultimately result in bone loss by osteolysis and subsequent implant failure. While a large number of studies have been undertaken to experimentally characterize wear rates of joint materials, the influence of surface parameters like residual stress, surface finish etc on the mechanisms governing damage nucleation is still not clearly understood. In the current study, we investigate the influence of residual stress on nucleation of nanoscale surface damage during fretting contact of an implant material.

In a total hip replacement there are two primary bearing surfaces, between the acetabular cup and femoral head and between the femoral stem and femoral head. The joint between the femoral stem and head is of concern since wear debris have been noted to form by fretting. Fretting is simply defined as when two contacting surface undergo small scale slipping. It is troublesome because it decreases the fatigue life of components and in the case of biomedical implants generates wear debris.

Biocompatibility determines the success of any implant design. Within the last several years an interest has arisen in testing the long-term biocompatibility of metallic implants. Materials commonly thought to have high biocompatibility (Ti alloys, Co alloys, Stainless Steels) have come under scrutiny primarily due to the release of wear particles that embed themselves into surrounding tissue. Independent work by Catelas et al.[1], Doorn et al. [2], and Fisher et al. [3] have revealed that the wear particles are typically tens of nanometers in diameter; and in the case of CoCrMo wear, Chrome oxide debris was the dominant type found in surrounding tissue [1, 2]. It is these small particles that Hallab and Jacob identify as the cause of three body wear, osteolysis, and toxicities [4]. In order to understand the wear debris generation it is necessary to understand the wear mechanism at the material interface.

Previous work on understanding the wear mechanisms of biomaterials has run the gamut from scratch testing to commercially available hip simulators. Catelas et. al used a commercially available hip simulator to perform long term testing on different Cobalt alloy combinations [1]. The test was stopped periodically to change the bovine serum, at which

point particles in the serum were analyzed. It was determined that the initial run in period occurred under 500,000 cycles at which point the majority of the alloys began to develop a steady state wear condition. More interestingly, Cobalt was rarely noted among the wear debris. It was concluded that the wear was primarily Chrome oxide debris. This supports an earlier work by Doorn [2] that discovered primarily Chromium traces in surrounding tissue from retrieved hip implants. This is entirely feasible considering recent experiments using XPS determined the oxide to be primarily Chrome Oxide and approximately 1.8nm thick [5]. Furthermore, Goldberg and Gilbert determined that when the passive layer is fractured, the oxide will repassivate on the order of milliseconds [6]. Using a modified equation for repassivation kinetics the researchers determine the thickness of the oxide was 1.86nm, which is in good agreement with Milosev and Strehblow. In addition, it was noted that approximately 6.4 GPa was required to elicit a current transient response (a measure of oxide repassivation by electrochemical means) thus suggesting Chrome oxide will not fracture from a single scratch at a lower stress level. Insight into the failure mechanism from previous studies eludes that the primarily chrome oxide passive layer is fractured and then rapidly repassivates in milliseconds with initial film failures occurring early in the life of the implant. Catelas work suggests the rapassivated film is primarily of the same composition since Chrome oxide debris is predominately found throughout the wear test duration (2 million cycles).

Contradictorily, Hallab et al. measured a larger ratio of Cobalt/Chromium from a serum solution surrounding a custom built hip simulator [7]. This discrepancy is probably due to the method of extracting the oxide debris. A 0.2μm filter was used to extract the wear particles; as determined by [1-3] this may be too large to capture a significant number of Chrome oxide debris (approximately 30-50nm in size). The primary goal of the study was not to measure wear particles however, but to determine the ideal material pairing. Material pairing is just one of many factors that have been known to affect fretting fatigue life. Other common variables include grain size, surface roughness, residual stress, loading amplitude/frequency, environment, and temperature.

Fretting wear is not unique to the biomaterials community. Fretting has been identified in turbine blades, ball bearings, as well as biomedical joint replacements. A

popular method to reduce fretting is to apply a surface treatment to the material. In practice residual stress may be induced in a material through surface treatments such as shot peening and nitriding. Studies incorporating surface treatments have met mixed results. One study examined Ti-alloy flats coated with TiN using PVD fretted against a Co-alloy counterface [8]. The researchers concluded that the hardened TiN coating held up very well however, Chromium debris was noted on the TiN coating after the test; indicating that the hardened coating accelerated the wear of the Co-alloy counterface. A study conducted to determine the ideal coating parameters found that compressive residual stress generally mitigated fretting fatigue damage [9]. Another study indicated that TiN coatings on tool steel did not affect the fretting rate during the life of the coating [10]. It was noted that after the coating was delaminated the wear rate was enhanced over the uncoated cases. Shot peening is another method of inducing compressive surface residual stresses. One troubling issue with shot peening is that tensile stresses are developed within the material to compensate for the compressive stress layer at the surface. To further complicate matters, research has demonstrated that the surface residual stresses will relax upon material removal [11, 12]. Hence, shot peening is not ideal for critical applications.

While compressive residual stresses are well accepted as being beneficial to wear resistance, a complete understanding of the residual stress effects on fretting wear is elusive. Residual stress and real area of contact are two parameters that are very difficult to control in traditional fretting test apparatus. The goal of this study is to overcome the limitations imposed by traditional long term testing fixtures with a novel experimental setup. This setup consists of a four point bending frame in conjunction with an atomic force microscope to apply residual and contact stresses respectively. The experiment is designed to mimic the onset of fretting damage by investing a single asperity contact (the AFM probe) oscillating over a controlled residual stress state. The materials, four-point bending frame, and experimental setup will be discussed in detail. Results of CoCrMo wear under varying contact loads and residual stresses will be displayed and discussed as it relates to macro scale phenomena.

3.3 Experimental Procedure

3.3.1 Material and Microstructure

The material used in this study is a cast Cobalt-Chromium-Molybdenum (CoCrMo) alloy as specified by ASTM F75. The samples were cut from canine femoral stem prosthesis (Biomedtrix, Las Vegas, NV) by electric discharge machining to form rectangular bars with dimensions of 1mm by 2mm by 25mm in the thickness, depth, and length respectively. Electric discharge machining was chosen to minimize processing induced residual stress affects so common in other forms of machining. The 1mm thickness of the beam was then mechanically polished by 1200 grit, 3 μm diamond suspension, 1 μm diamond suspension, and finally with a 0.05 μm colloidal silica (Buehler, Lake Bluff, IL) suspension to a mirror finish. AFM measurements on the polished side indicate that the initial surface follows a Gaussian distribution with skewness approximately zero (-0.1 to .08) and kurtosis of approximately 3 (2.8 to 3.2). The root mean square (RMS) roughness ranges from 0.5nm to 2nm on 10μm scans, indicating a very smooth initial surface. Several samples were etched with a solution of 20mL HCl, 10mL HNO_3^-, and 3g $FeCl_3$ [13] to determine the average grain size. The microstructure reveals large grains (Fig. 1), typically on the order of a hundred microns, with very few carbides present.

3.3.2 Four-point bending frame

A four point bending frame was designed in order to apply controlled "residual stress" to the sample. The four point bending frame (c-frame) consists of a 304 stainless steel c-clamp, base, and hardened steel pin gages (Meyers Gage, South Windsor, CT) to act as rollers (Fig. 2). The sample is placed in-between the clamp and base so that the rollers force the c-clamp to open, while a capacitance gage (Capacitec, Ayer, MA) monitors the deflection of the free end of the c-clamp. The opening of the c-clamp exerts a force onto the rollers creating a uniform bending state at the center of the sample. The amount of force supplied by the c-clamp is simply a measure of the deflection at the end of the clamp and that of the two rollers in the center. The deflection-force relationship of the clamp was calibrated by a dead weight method. The deflection was monitored with the capacitance gage while

calibration weights were hung from the center of the clamp, producing a calibration curve. A linear least squares fit was applied to the average of five calibration trials, the data reveals a nice linear relationship with a slope of 186.1 μm/lb. The deflection experienced by the rollers is nearly insignificant, only accounting for about 2-3% of the error in the residual stress calculation. The error analysis will be discussed in more detail in the following sections. The resulting residual stress values only depend on the geometry of the sample, deflection of the clamp, and the distance away from the edge of the sample; the material properties are inconsequential.

3.3.3 Atomic Force Microscope

The atomic force microscope (AFM) used in this study is a Dimension 3100 with Nanoscope IV controller (VEECO Instruments, Woodbury, NY). Silicon nitride (Si_3N_4) cantilevers with a reflective gold backside coating (DNP-S Veeco) and a manufacturer's spring constant of 0.58 N/m were used in the present study. AFM probes are batch manufactured and subject to variations in the thickness of the cantilever, leading to spring constants far different than the nominal value suggested by the manufacturer. To account for this, each cantilever's spring constant was determined by monitoring the deflection of the cantilever against a hard substrate (SiC) as well as a reference cantilever with known spring constant (Veeco). The cantilever and substrate act as two springs in series and the spring constant of the experimental cantilever can be deduced by equation 1 [14].

$$k_{cantilever} = \frac{(\delta_{SiC} - \delta_{RC})}{\delta_{RC}} * (k_{RC}) \qquad (1)$$

In equation 1 'δ' is the deflection and 'RC' is the reference cantilever. This calibration was preformed prior to each experiment. In addition, the probe radius was obtained by inverse imaging the probe over a calibration grating that has silicon spikes with radii of curvature less than 10nm (TGT01 Micromasch, Wilsonville, OR). When the AFM tip (radius of curvature > 30nm) is scanned across the characterizer the image is actually of the tip itself. With this image the radius of curvature of the tip may be monitored for wear before and after each experiment.

3.3.4 Experimental Procedure

The CoCrMo sample is loaded into the c-frame by inserting the sample and rollers while the free end deflection of the clamp is monitored with the capacitance gage. The change in displacement of the clamp is divided by the calibration factor (186.1 μm/lb) to determine the force exerted through the clamp onto the rollers. In order to locate a given residual stress state along the cross-section of the beam it is necessary to determine the distance from the edge of the beam. This is accomplished by using an optical camera with a well-characterized pixel resolution.

The CoCrMo sample is imaged by a Sony XCD-SX910 FireWire camera equipped with an optical microscope (VZM 1000i, 100-400X Magnification, Edmund Optics, Barrington, NJ). Identifiable features, such as scratches or adhesive wear pits from polishing, are located and their distance from the sample edge is measured in pixels. The pixel value is then converted to metric units by images of a stage micrometer taken at the same resolution. These features are then used as markers when determining a testing location with the AFM's optical camera.

The loaded sample is then placed underneath the AFM and the optical camera on the AFM relocates the area previously identified. The tests are conducted at the same distance away from the edge but also away from the feature to avoid adverse affects due to geometry or additional residual stress. The sample was studied at various contact forces and residual stress states (Fig 4). Figure 4 depicts the area in which testing would be carried out along the beam. The upper right inset demonstrates that the sample will be in a compressive state at the top of the beam and will vary through a zero stress state at the center to a tensile state at the lower portion of the beam. For five residual stress states five different loading conditions were studied (upper right inset Fig 4). The lower inset depicts the loading action created by the AFM tip on a tensile residual stress state.

All tests were preformed in an ambient environment with a relative humidity of 50%. Once the residual stressed area was located with the AFM's camera a 5 μm scan was taken at 1-2 nN and 2 Hz. The wear test was then preformed at the center of the 5 μm scan on an area of 2 μm by 500 nm. The tip was rastered across this area at 5 Hz for each defined load for 15

minutes (ISO 7206-7 "Endurance performance of stemmed femoral components without application of torsion" considers 5-10Hz acceptable for accelerated testing). Under these conditions each scan line would be covered approximately 70 times along the slow scan axis (500nm dimension). After 15 minutes the scanning parameters were adjusted back to 5 μm, 2 Hz, and 1-2nN to capture the final image. After each test the probe radius was measured using the characterizer. Generally, a single probe was used to conduct four tests at 75, 50, 25, and 1-2nN of force.

3.4 Results and Discussion

3.4.1 Wear Rate Measurement

The initial surface of the sample was very smooth; however, even small changes in the surface roughness such as scratches or adhesive tear out pits from polishing are unavoidable. In order to minimize the effects of initial surface imperfections and calculate the wear depth accurately, the initial and final 5μm images obtained on the AFM were aligned and subtracted using the Matlab image processing toolbox as well as some custom written code. The image processing toolbox allows for the selection of identifiable features on each image, termed control points. From these control points the final image is rotated and translated until it overlaps the initial image. For instance, figure 4a displays the initial image of the 5μm test area while figure 4b displays the final image after 15 minutes of scratching. Figure 4b is then translated to align with figure 4a; the final image is subtracted from the initial image resulting in figure 4c. The dashed box in figure 4c indicates the area displayed in figure 4d. The resultant subtracted image (fig. 4c) displays very minor changes in the surface roughness. A quantitative wear depth is measured by subtracting average trench height from the average height of the surrounding surface.

3.4.2 Contact Stress Estimation

The average contact pressure was determined from a Hertzian solution. The probe's radius of curvature was monitored before and after each experiment. A relative radius of curvature was determined by fitting parabolas to the reverse image of the probe. To find the principal radii of curvatures, the probe image was projected in the x-z plane and the

maximum points were determined. This process was then repeated at 90 degrees in the y-z plane. Quadratic functions were determined by a linear least squares fit to the two data sets; it was from these quadratic functions that the probe radii were determined. The radius of curvature used in the Hertzian solution was then determined to be the average of the relative radius of curvature before and after the experiment. The load on the probe is well characterized from the deflection signal off of the calibrated experimental cantilever. The properties of CoCrMo [13]and Si_3N_4 [15] were taken as E_s= 248 GPa, E_p=310 GPa and ν_s= ν_p= 0.3 for elastic modulus and Poisson's ratio respectively. Where 's' denotes substrate (CoCrMo) and 'p' denotes the probe (Si_3N_4). Since the experiment was conducted in an ambient environment some adhesive forces due to an adsorbed water layer on the sample are expected. These were accounted for by monitoring the force deflection curves produced during the experiments. The adhesive forces were then added to the applied loading in the Hertzian solution.

3.4.3 Error Estimation

The uncertainty in the residual stress values was conservatively estimated by taking into account the deviations of the force value discussed earlier, the geometry of the sample, and the camera used in determining the distance from the edge of the sample. The error attributed to the high-resolution camera comes from the images of the stage micrometer. The grayscale transition produced by the ticks on the stage micrometer was determined to be two pixels for lower resolutions and around four pixels at higher resolutions. This corresponds to approximately 1-2 μm deviations in the distance from the edge. The primary source of error arises from the geometry of the sample; in beam analysis the stress varies by the thickness cubed times the depth. The dimensions of the sample were measured by a digital caliper (Mitutoyo, Aurora, IL) with resolution of +or- 10μm. This error was incorporated into the estimation calculation for residual stresses.

The error estimation of the wear depth was preformed by taking several measures of the mean height within and outside the trench area. The error bars are plus and minus one standard deviation from the change in surface height. The range of contact stresses listed in the legend is also a result of error analysis. The maximum and minimum contact pressure

was determined from deviations in the change of the relative radius of curvature. These deviations are the result of different initial probe radii. The variations of load caused by the calibration method of the cantilever were not accounted for since the load varies proportionally to the stress by a power of 1/3, whereas the radius of curvature is inversely proportional to the contact stress by a power of 2/3 and will dominate the term. The amount of error caused by the calibration procedure is assumed to be small since the spring constant was similar across all of the cantilevers used.

As mentioned previously, the geometry of the AFM tip was characterized before and after each experiment. It is interesting to note the wear rate of the AFM tip is fairly consistent throughout all of the tests. The change in the relative radius of curvature was approximately 3-6 nm after four loading trials of 75nN, 50nN, 25nN, 1-2nN. Typically the largest change was noted after the 75nN loading condition where the tip sustained the most damage. Subsequent trials at 50nN, 25nN, and 1-2nN produced minor changes in the tip geometry.

3.4.4 Discussion

All experimental data was taken under ambient conditions with the relative humidity ranging between 48-53% inside the AFM chamber. Figure 5 depicts the trench depths as a function of the normalized residual stress. The plot displays four series indicating the amount of nominal Hertzian pressure applied by the AFM probe. The lowest loading case (approximately 800MPa) did not produce a discernable trench on any of the residual stress states. It is noted that the first detectable trench appears at a contact stress greater than 3MPa for any residual stress state. The three larger loading cases all display an increasing trend in trench depth as the residual stress state changes from tensile to compressive.

The difference in the trench depths between the compressive and tensile side should not be contributed to a change in hardness of the CoCr alloy produced by the residual stress. Nano-indentation experiments preformed by Tsui, Pharr and Oliver [16] reveal that preexisting stress in a material has an insignificant effect on the hardness value. Schall and Brenner [17] received similar results when modeling nano-indentation of pre-stressed material using a MD simulation. In addition, the wear of the AFM tip before and after each

experiment argues strongly against a differential hardness across the sample. From monitoring the wear rate before and after each experiment, no significant difference is discernable between the tensile and compressed cases. The compliance of the substrate should be directly proportional to the wear on the tip. From this it is concluded that the material response is similar on all regions of the beam.

The trench depths plotted in Fig. 5 are the result of two competing processes, delamination and repassivation. The failure of the oxide layer is hypothesized to proceed by delamination of the passive film followed by rapid repassivation continuing in a cyclic manner. As the AFM tip rasters across the surface, the high contact stress damages the oxide film and the underlying substrate. The residual stress within the material will dictate the proportion of damage sustained by the film and the substrate. As the oxide is removed or damaged the underlying anodic materials (Chromium, Molybdenum, Cobalt) will voraciously begin to repassivate, forming a new oxide layer. Previous studies indicate that the repassivation process takes place much faster than the AFM can scan (ms-sec), thus it is not possible to measure the repassivation rates with an AFM alone.

The noticeable linear trend between residual stress and trench depth in Fig. 5 is the result of residual stress effects on the repassivation, delamination, or both. On the repassivation side, residual stress may either affect the oxidation kinetics by retarding/accelerating film growth or repassivating the metal with different concentrations of oxide. For instance, Chrome oxide is the dominant oxide on CoCrMo however it is probable that Cobalt oxide may repassivate the surface in higher concentrations depending on the stress state. Milosev et al. [18] noted that by changing the potential difference across a Ti-alloy the composition of the passive layer will vary. Yu and Suo have demonstrated that residual stress plays a significant role in surface reaction kinetics [19]. It was determined that residual stress would either affect the reaction by dominating the mobility of the reaction (a linear effect) or the driving force (a quadratic effect). The results demonstrate a marked linear dependence between trench depth and residual stress. However, the residual stress may not only affect the oxide repassivation. The delamination of the film may also be influenced by the residual stress state.

Work by He et al. investigated the nature of cracks reaching interfaces between two dissimilar elastic materials under a residual stress field. This situation is precisely what we are faced with when dealing with oxide coated metals. A crack in this situation has three probable paths: 1) To penetrate the interface and dissipate the energy in the second material; 2) To propagate along the interface, debonding the two materials; 3) To die at the interface. The path selection was determined to be strongly influenced by the residual stress state. The researchers have developed relationships between the elastic moduli, residual stress state, and ratio of relative energy release rates. The ratio of relative energy release rates determines whether a crack is more likely to propagate along the interface or penetrate into the material. For the case of a stiffer oxide coating a ductile material this suggests that the propensity for a crack to penetrate the interface into the ductile substrate is nearly 3 times greater for a tensile stress than a compressive stress. Other work by Ye and Komvopoulos [20] demonstrate that the size of the plastic zone created by a moving indenter is largely dictated by the residual stress in the material. The finite element model developed incorporates a rigid film attached to a ductile substrate. Residual stress is applied to the film causing the opposite stress effect within the substrate. A tensile stress in the substrate permitted more energy dissipation allowing the film to undergo little damage. A compressive residual stress in the substrate hindered the energy dissipation, creating a small plastic zone. The film in this case was subjected to more damage since it was required to absorb more of the energy dissipation. In each of these studies it is apparent that compressive residual stress retards the amount of energy dissipated into the substrate, making it more likely for the film to be damaged. Figures 6 and 7 illustrate this by depicting a differing plastic zone size depending on the residual stress state. For the case of the compressive residual stress the smaller plastic zone size, hence less energy dissipation, will promote damage/delamination of the oxide layer. The tensile residual stress will permit a larger plastic zone, more energy dissipation into the substrate, thus preserving the integrity of the oxide layer.

At this time it is believed that the residual stress induced delamination of the oxide is dominating the wear mechanism. To illustrate this Figures 8 and 9 displays the AFM scan after 15 minutes of fretting action at the same applied contact pressure. Figure 8 is compressively stressed at 90 MPa while Fig 9 is under a tensile stress of 75 MPa. The wear

pileups in the middle of each image give an indication of the amount of oxide debris produced. The compressive case (Fig. 8) has much larger pileups than the tensile case (Fig. 9) thus indicating more wear. This trend of larger pileups on the compressive side is consistent throughout the tests.

Initially, it seems counterintuitive that compressive stress facilitates the wear of the oxide layer, especially in light of the previous experiments that suggest compressive stress is beneficial at mitigating the wear. However, it must be taken into context that this experiment only investigates the initial damage mode under fretted loading. In addition, recent studies have noted beneficial effects produced by the presence of oxide wear debris. A previous study investigating the role of oxide particles on wear determined that oxide debris may provide a beneficial or harmful effect [21]. The dual nature of the oxide debris was dependent on the loading and slip amplitude. For smaller slip amplitudes, around 50 μm, it was found that oxide debris protected the surface by acting as a third body and then turning into a compacted oxide layer inhibiting wear. Endo and Marui [22] found that steels will exhibit the same behavior, reporting that wear debris adhered to the surface, inhibiting wear. Barril et al. [23] conducted a ball on flat fretting test equipped with an electrochemical cell. The researchers noted sudden decreases in the coefficient of friction as an increase in current was detected. The current increases were thought to be the ejection of wear particles from the contact. Benrabah et al [11] found that wear debris produced during fretting of shot peened samples was beneficial in protecting the two contacting bodies. The researchers hypothesized that the wear debris was able to accommodate the relative velocity, thus supporting Barril et al. observation of decreased friction forces.

The recent experiments may provide some insight into the beneficial nature of residual stresses in long term testing. During the initial run in period compressive residual stresses facilitate the delamination of the native oxide under fretting contact. As the oxide is delaminated, the underlying metal will repassivate forming new oxide. The nanoscale wear debris generated from the delamination of the oxide acts as a solid lubricant until it is compacted back into the existing oxide, strengthening it, or ejected from the contact area.

3.5 Conclusion

- Conducted nano-scale investigation to identify the influence of surface residual stress on wear rate of cobalt-chromium alloy
- Contact pressure greater than 800 MPa is required to initiate wear of Co-Cr alloys in single asperity contact.
- Tensile stress suppresses oxide damage while compressive stress enhances the damage process.

The exact nature of residual stress during fretting fatigue is still somewhat elusive due to its complex synergistic behavior. Residual stress may influence the repassivation of the oxide and/or the delamination of the oxide. The current discussion is primarily centered on the latter argument since it is difficult to hypothesize on the nature of the repassivation given the current setup. Future studies will investigate this behavior in different environment in an attempt the extract the role of residual stress in the repassivation process.

3.6 Acknowledgements

The authors would like to acknowledge helpful discussions with Dr. Sundararajan. As well as, financial support through Special Research Initiation Grant of Iowa State University.

3.7 References

[1] I. Catelas, J. D. Bobyn, J. B. Medley, J. J. Krygier, D. J. Zukor, and O. L. Huk, "Size, shape, and composition of wear particles from metal-metal hip simulator testing: Effects of alloy and number of loading cycles," 2003.

[2] P. F. Doorn, P. A. Campbell, J. Worrall, P. D. Benya, and H. A. Mckellop, "Metal wear particle characterization from metal on metal total hip replacements: Transmission electron microscopy study of periprosthetic tissues and isolated particles," *Journal of Biomedical Materials Research*, vol. 42, pp. 103-111, 1998.

[3] J. Fisher, X. Q. Hu, T. D. Stewart, S. Williams, J. L. Tipper, E. Ingham, M. H. Stone, C. Davies, P. Hatto, J. Bolton, M. Riley, C. Hardaker, G. H. Isaac, and G. Berry,

"Wear of surface engineered metal-on-metal hip prostheses," *Journal of Materials Science-Materials in Medicine*, vol. 15, pp. 225-235, 2004.

[4] N. J. Hallab and J. J. Jacobs, "Orthopedic implant fretting corrosion," *Corrosion Reviews*, vol. 21, pp. 183-213, 2003.

[5] I. Miloslev and H. H. Strehblow, "The composition of the surface passive film formed on CoCrMo alloy in simulated physiological solution," *Electrochimica Acta*, vol. 48, pp. 2767-2774, 2003.

[6] J. R. Goldberg and J. L. Gilbert, "Electrochemical response of CoCrMo to high-speed fracture of its metal oxide using an electrochemical scratch test method," *Journal of Biomedical Materials Research*, vol. 37, pp. 421-431, 1997.

[7] N. J. Hallab, C. Messina, A. Skipor, and J. J. Jacobs, "Differences in the fretting corrosion of metal-metal and ceramic-metal modular junctions of total hip replacements," *Journal of Orthopaedic Research*, vol. 22, pp. 250-259, 2004.

[8] J. A. Hendry and R. M. Pilliar, "The fretting corrosion resistance of PVD surface-modified orthopedic implant alloys," *Journal of Biomedical Materials Research Part B: Applied Biomaterials*, vol. 58, pp. 156-166, 2001.

[9] Y. Fu, J. Wei, and A. W. Batchelor, "Some considerations on the mitigation of fretting damage by the application of surface-modification technologies," *Journal of Materials Processing Technology*, vol. 99, pp. 231-245, 2000.

[10] H. Morbacher, B. Blanpain, J. P. Celis, J. R. Roos, L. Stals, and M. V. Stappen, "Oxidational wear of TiN Coatings on tool steel and nitrided tool steel in unlubricated fretting," *Wear*, vol. 188, pp. 130-137, 1995.

[11] A. Benrabah, C. Langlade, and A. B. Vannes, "Residual Stresses and fretting fatigue," *Wear*, vol. 224, pp. 267-273, 1999.

[12] N. W. Bonner, R. C. Wimpory, G. A. Webster, A. T. Fry, and F. A. Kandil, "Measurement of residual stress through a spot peened surface subjected to succesive material removal," *Materials Science Forum*, vol. 404-407, pp. 653-658, 2002.

[13] A. C. Fraker, "ASM Handbook," in *Corrosion of Metallic Implants and Prosthetic Devices*, vol. 13, pp. 1324-1335.

[14] M. Tortones and M. Kirk, "Characterization of application specific probes for SPMs," *SPIE*, vol. 3009, pp. 53-60, 1997.

[15] S. P. Ho, R. W. Carpick, T. Boland, and M. LaBerge, "Nanotribology of CoCr-UHMWPE TJR prosthesis using atomic force microscopy," *Wear*, vol. 253, pp. 1145-1155, 2002.

[16] T. Y. Tsui, W. C. Oliver, and G. M. Pharr, "Influences of stress on the measurement of mechanical properties using nanoindentation: Part I. Experimental studies in an aluminum alloy.," *Journal of Materials Research*, vol. 11, pp. 752-759, 1996.

[17] J. D. Schall and D. W. Brenner, "Atomistic simulation of the influence of pre-existing stress on the interpretation of nanoindentation data," *Journal of Materials Research*, vol. 19, pp. 3172-3180, 2004.

[18] I. Milosev, M. Metikos-Hukovic, and H. H. Strehblow, "Passive film on orthopaedic TiAlV alloy formed in physiological solution investigated by X-ray photoelectron spectroscopy," *Biomaterials*, vol. 21, pp. 2103-2113, 2000.

[19] H. H. Yu and Z. Suo, "Stress-dependent surface reactions and implications for a stress measurement technique," *Journal of Applied Physics*, vol. 87, pp. 1211-1218, 2000.

[20] N. Ye and K. Komvopoulos, "Effect of residual stress in surface layer on contact deformation of elastic-plastic layered media," *Journal of Tribology*, vol. 125, pp. 692-699, 2003.

[21] A. Iwabuchi, "The Role of Oxide Particles in the Fretting Wear of Mild-Steel," *Wear*, vol. 151, pp. 301-311, 1991.

[22] H. Endo and E. Marui, "Studies on fretting wear: influence of rubbing surface materials and some considerations," *Wear*, vol. 253, pp. 795-802, 2002.

[23] S. Barril, N. Debaud, S. Mischler, and D. Landolt, "A tribo-electrochemical apparatus for in vitro investigation of fretting-corrosion of metallic implant materials," *Wear*, vol. 252, pp. 744-754, 2002.

3.8 Figure Captions

Fig. 1 Microstructure of the CoCrMo rectangular beam. Note that the grain size is relatively large with several grains reaching hundreds of microns in diameter.

Fig. 2 The four point bending setup. The main components are a c-clamp, base, capacitance probe, rollers, and a rectangular sample.

Fig. 3 The lower left image displays the loaded clamp. The upper right inset depicts the range of residual stress values and locations for testing various contact loads (white boxes). Each white box depicts a testing location.

Fig. 4 A) The initial 5 μm scan. B) The final 5 μm scan after 15min of scratching. C) The resultant image after the initial image is subtracted from the final image. D) A zoomed in image of the white dashed box in 5C. The scale bar to the left applies to 5A-C while the right hand scale bar is for image 5D.

Fig. 5 Average trench depth plotted against the normalized residual stress value.

Fig. 6 Illustration of the damage zone caused AFM probe with a substrate in compressive residual stress

Fig. 7 Illustration of the damage zone caused AFM probe with a substrate in tensile residual stress

Fig. 8 AFM scan of the 5μm area after 15 minutes of fretting. This area is under 90MPa of residual compressive stress

Fig. 9 AFM scan of the 5μm area after 15 minutes of fretting. This area is under 75Mpa of residual tensile stress.

Fig. 1

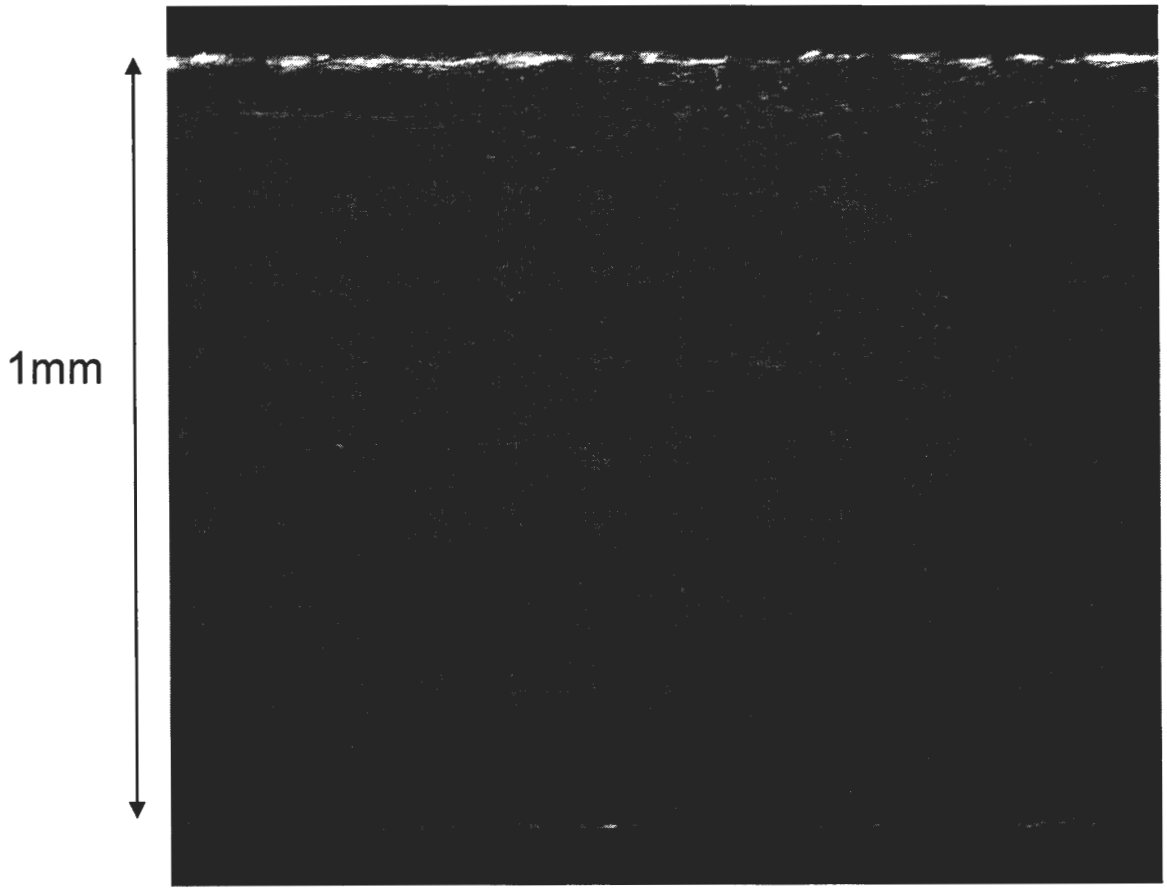

Fig. 2

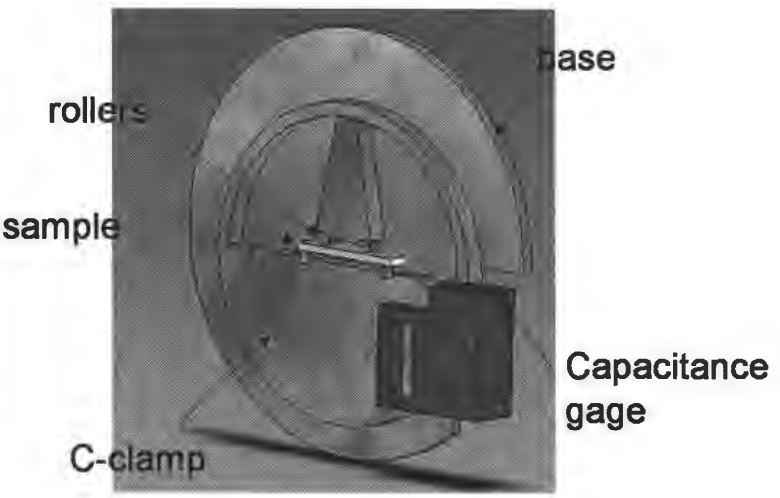

Fig. 3

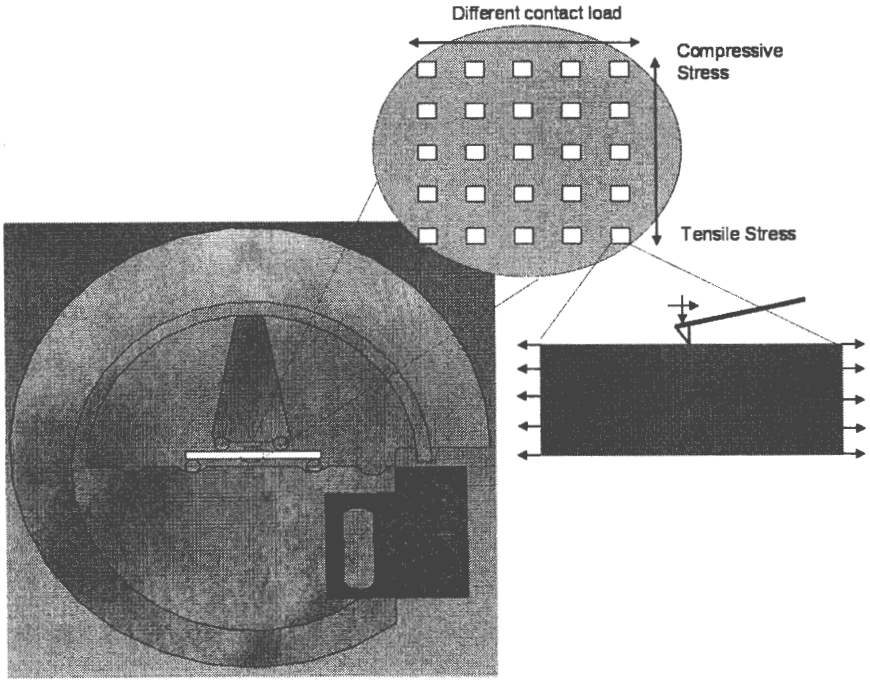

Fig. 4

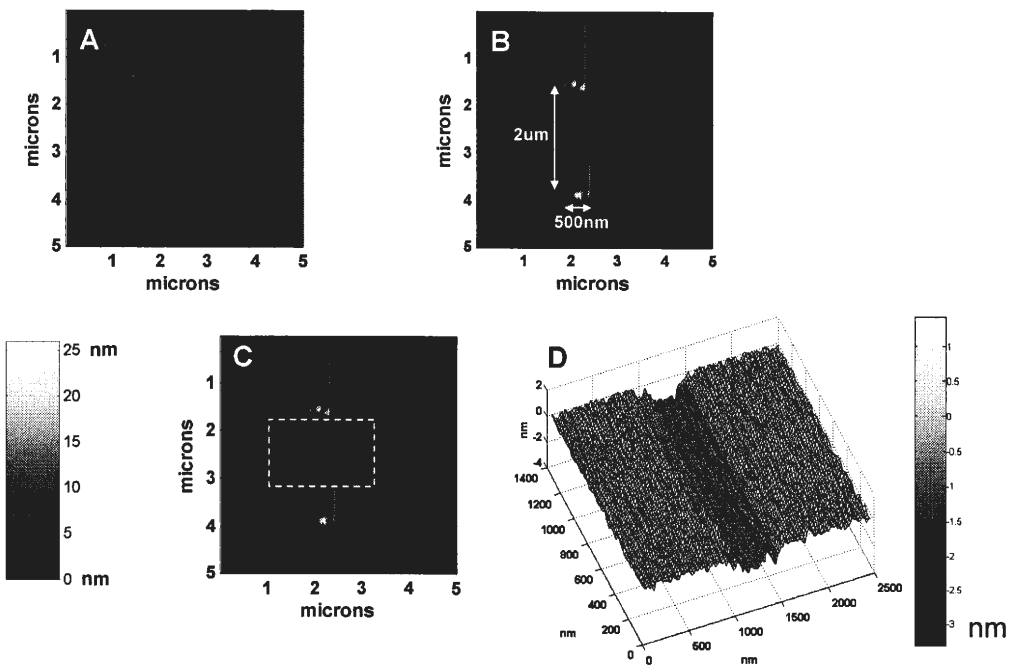

Fig. 5

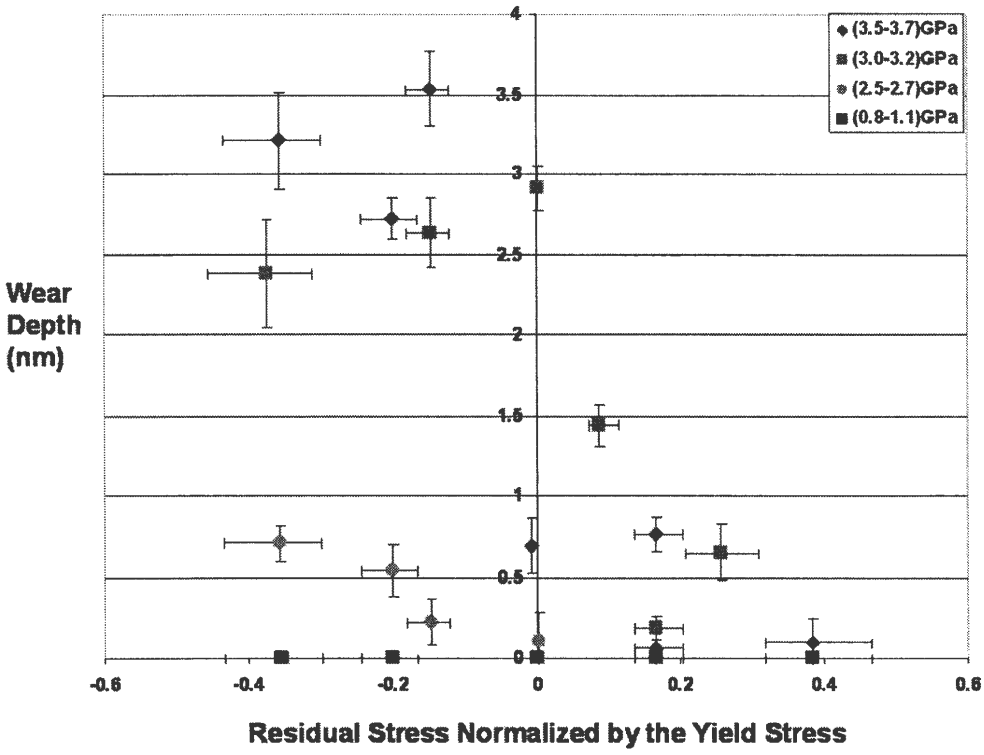

Fig. 6

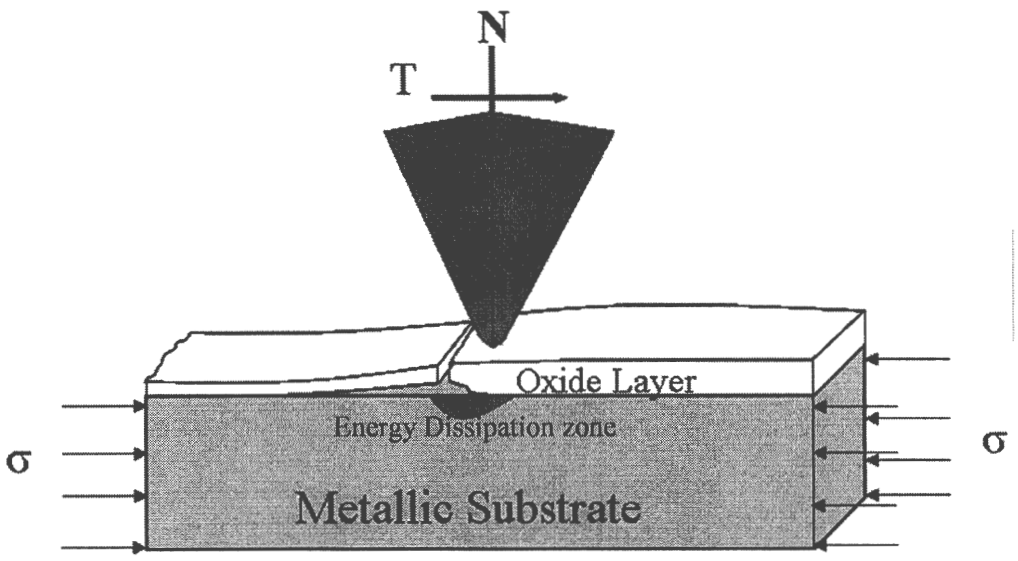

Fig. 7

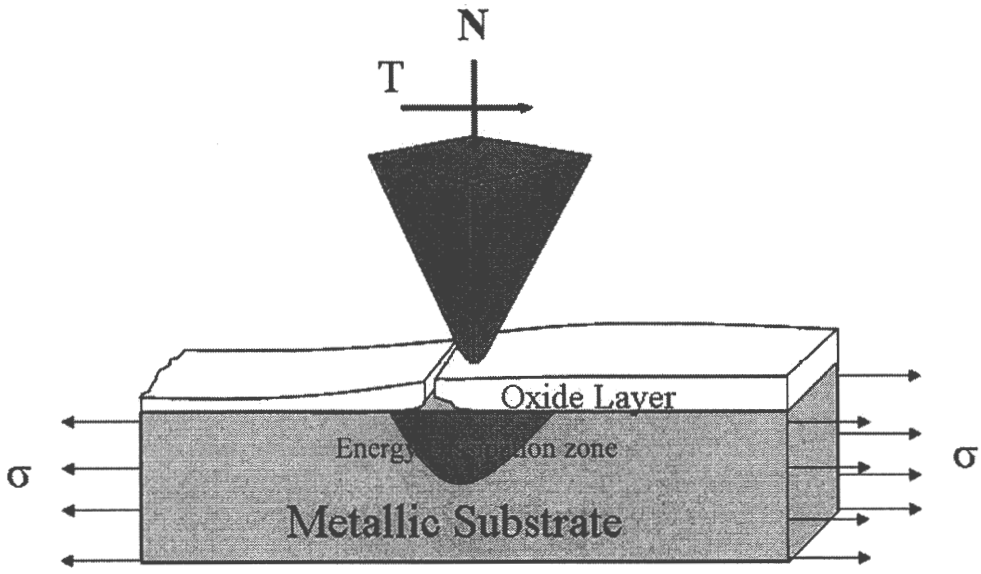

Fig. 8

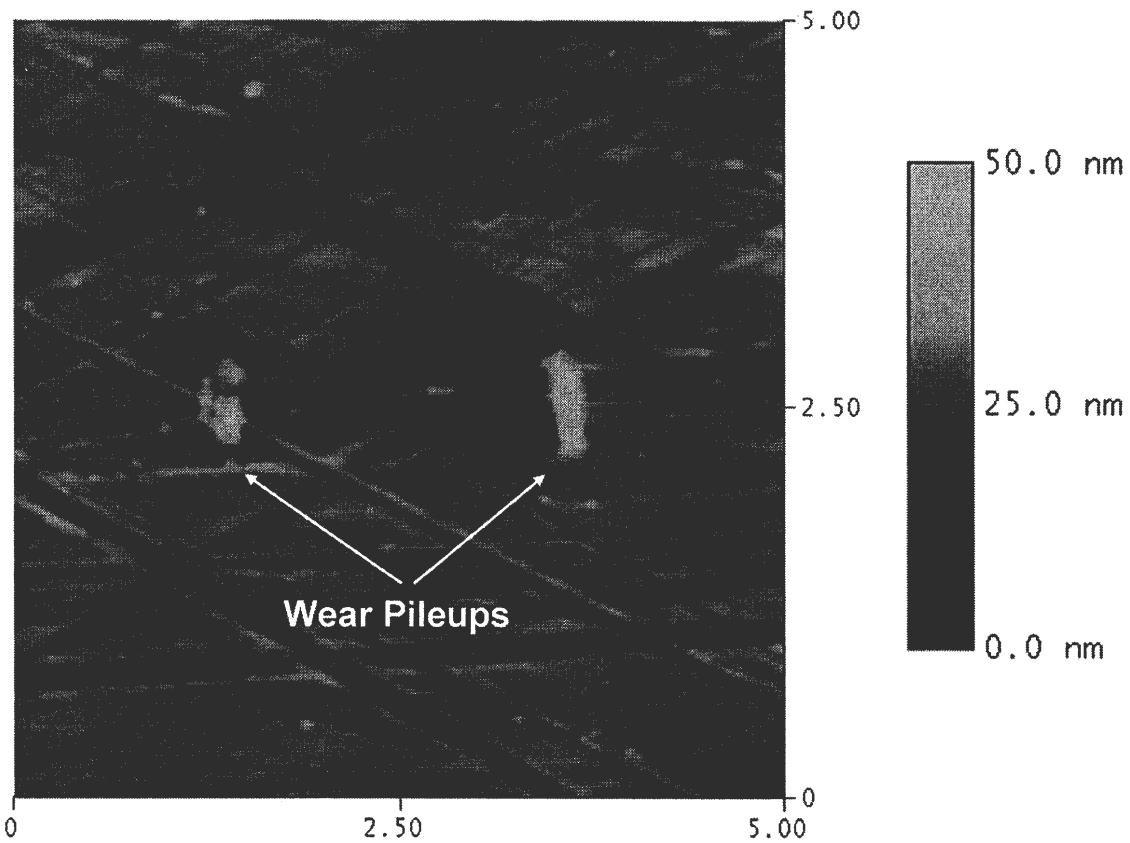

Fig. 9

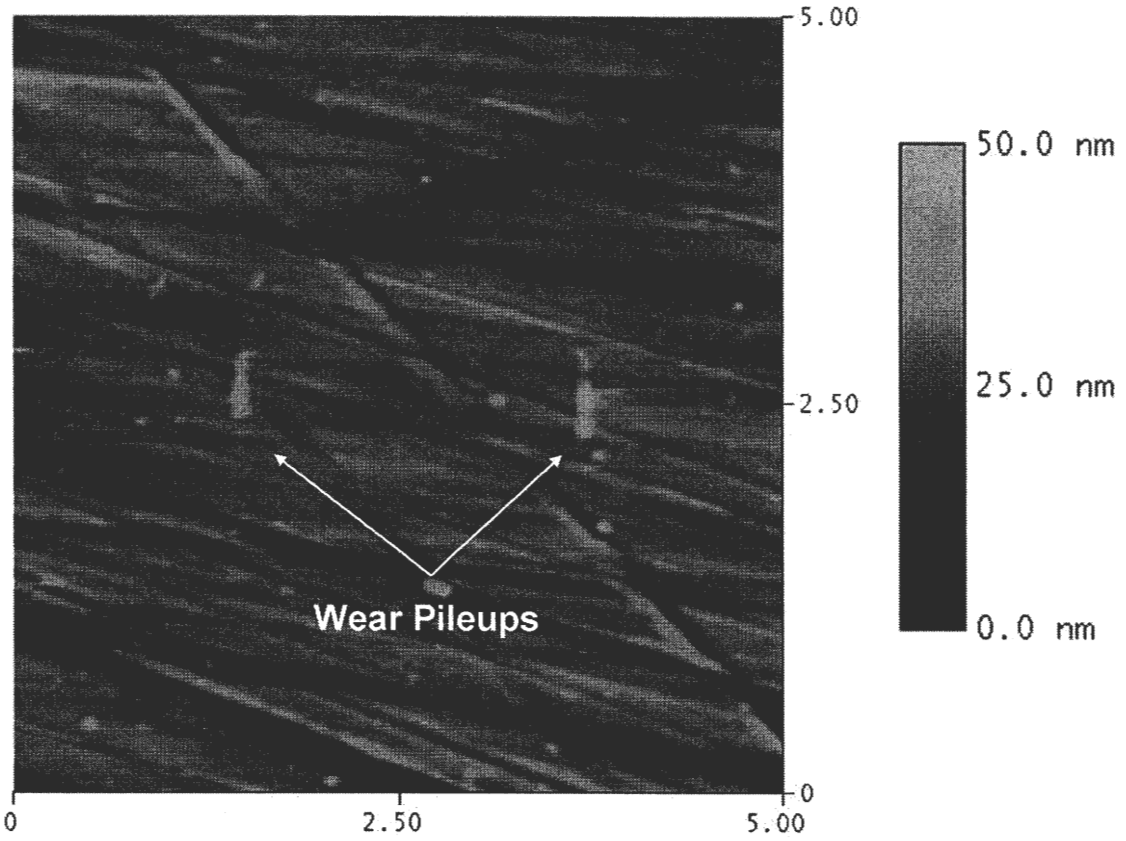

Chapter 4. Mechanical load assisted dissolution of metallic implant surfaces: Influence of contact loads and surface residual stresses

A paper to be submitted to the journal Biomaterials

Andrew Mitchell, Pranav Shrotriya
Department of Mechanical Engineering, Iowa State University, Ames, Iowa 50011, USA

4.1 Abstract

Mechanical load assisted dissolution is identified as one of the key mechanism governing material removal in fretting corrosion of biomedical implants. Repeated contact of biomedical implants in a corrosive physiological environment leads to fretting corrosion resulting in formation of soluble and particulate debris that may induce a cascade of inflammatory events or failure of the implant. While it is well known that stress affects the dissolution rate of material the exact mechanisms governing stress-assisted dissolution are still not well understood. In order to identify the governing mechanism, dissolution of a stressed metallic surface subjected to single asperity contact is investigated. For this study, specimens are mounted in four point bending configurations such that a range of stress levels are applied to the specimen surface. The testing configurations are designed for easy accessibility to facilitate in-situ mechanical stimulation and imaging by Atomic Force Microscope (AFM). Using the tip of an atomic force microscope (AFM) as a well characterized "asperity," controlled contact forces are applied to mechanically stimulate the loaded specimen surface in ambient and oxidizing environments. This would be analogous to a wear particle (the AFM probe) coming into contact with the stressed surface of an implant or work piece. The material removed is measured to determine the dissolution rate as a function of applied surface stress and contact loads. In addition, comparisons are made from previous observations that identify key mechanisms in the failure process.

Keywords: Residual Stress, Biomaterials, CoCrMo, Dissolution, Corrosion

* corresponding author: Tel: +1 515-294-9719; email: shrotriy@iastate.edu

4.2 Introduction

The total hip replacement is a coupling of three primary modular components. It consists of a femoral head, femoral stem, and acetabular cup. The modular design has supplanted previous conformal designs since it allows a great deal of latitude for surgeons to customize the implant for a particular patient while at the same time maintaining a small inventory of components. While convenient, the modular design consists of two primary bearing surfaces which have come under scrutiny by the biomedical community. The first bearing surface is between the acetabular cup and the femoral head. This generally comprises a metal-polymer, ceramic-ceramic, ceramic-polymer, or metal-metal contact. The second bearing surface is between the femoral head and femoral stem. These two components attach by interlocking tapers (Morse tapers). The contact materials here are either metal or ceramic with the variation coming from the choice of femoral head, the femoral stem is always metallic. The junction between the head and the stem is of particular interest since previous studies have reported wear debris generation due to fretting corrosion [1-5]. The wear debris has been identified as the cause of such problems as osteolysis, inflammation, and implant loosening all of which may lead to a costly revision surgery.

Gilbert et al. [6] studied 148 retrieved modular hip protheses to determine a failure mechanism. The femoral head and stem were examined for signs of corrosion. A mechanically assisted crevice corrosion hypothesis was put forth as a means for explaining the failure mechanism of the metallic components. The hypothesis assumes a classic crevice corrosion environment where interfacial shear stresses cause local fracture of the protective oxide film covering biomedical implant alloys. The underlying metals will then spontaneously react and repassivate the oxide layer. This process of fracture and repassivation continues producing a differential aeration in the crevice. The differential aeration is followed by subsequent drops in the pH and the creation of a hostile HCl environment. Ultimately, the pH will decrease below the stability point of Chrome Oxide not permitting the metal to repassivate. At this point the underlying metal will undergo aggressive local attacks where the oxide layer has been fractured.

The hypothesis of mechanically assisted dissolution has been well accepted by the biomedical community. While the researchers claim that fracture of the oxide takes place locally, it has been applied to many macro-scale experiments. The actual mechanism of asperity level oxide fracture and subsequent repassivation is still enigmatic. For instance, surface residual stresses are assumed to be present due to continuous asperity level contacts. Residual stress effects on oxide fracture are unclear; however the nature of residual stress on the dissolution of material is an ongoing area of research outside of the biomedical community.

A classical example of stress-assisted dissolution is that of stress corrosion cracking (SCC). This is essentially a premature brittle failure of a susceptible alloy that has some form of tensile stress subjected to a corrosive environment. The understanding of residual stress on dissolution has increased greatly since SCC experiments; gaining significant ground with the advent of experimental equipment with nanoscale resolution, namely the AFM. Kim et al. [7] developed a technique termed surface roughness-evolution spectroscopy. This technique describes a manner to measure surface residual stresses by simply monitoring the surface roughness evolution with an AFM during etching. Yu and Suo [8] have developed a theory based on the work of Kim et al. [7] and Aziz et al. [9] that describes the role of residual stress in chemical reaction kinetics. Two different hypothesis of stress influence of dissolution reaction rate were proposed:

i) Driving Force: Strain energy increases energy density of surface, there by increasing the reaction rate , resulting in a "quadratic" dependence
ii) Mobility: Stress state perturbs the mobility of surface chemical reaction rate resulting in a linear dependence on reaction rate

The exact mechanism (driving force or mobility) affected by surface stresses is not generally known and may be environmentally and reaction dependent. Aside from dissolution modified by residual surface stresses the contact loads themselves may affect the dissolution rate. Work by Park et al. [10] demonstrated that $CaCO_3$ dissolution is affected by scanning of an AFM tip. It was demonstrated that an applied load dependent dissolution rate was consistent to the activation volume underneath the tip. In order to clarify the role of surface

residual stresses and contact loads in the mechanically-assisted dissolution model for CoCrMo a new experimental technique has been developed.

In order to understand the nature of the local oxide failure on CoCrMo an AFM tip is used as a single surface asperity contacting the substrate. The AFM offers the unique ability to apply well characterized loads while at the same time knowing the real area of contact. Surface residual stresses are applied through a custom built four-point bending frame to be used in conjunction with the AFM. The entire setup is capable of testing specimens in ambient or aqueous environments.

In the current experiment, trends between the wear rates and environment, surface stress, and loading condition are drawn. In the following sections an overview of the experimental setup and procedure will be given. The following discussion will augment the well accepted mechanically-assisted dissolution hypothesis by providing an understanding of asperity level behavior.

4.3 Materials and Equipment

4.3.1 Samples

The material used in this study is a cast Cobalt-Chromium-Molybdenum (CoCrMo) alloy as specified by ASTM F75. The samples were cut from canine femoral stem prosthesis (Biomedtrix, Las Vegas, NV) by electric discharge machining to form rectangular bars with dimensions of 1mm by 2mm by 25mm in the thickness, depth, and length respectively. Electric discharge machining was chosen to minimize processing induced residual stress affects so common in other forms of machining. The 1mm thickness of the beam was then mechanically polished to a mirror like finish. The sample is then loaded into the four point bending frame.

4.3.2 Four point bending frame

The four-point bending frame (c-frame) is designed to apply varying levels of residual stress throughout the sample. Figure 1 displays a bird's eye view as well as an isometric view of the c-frame. The sample along with four rollers are placed in-between the c-clamp and the extrusion on the base. The rollers, which are modified pin gages (Meyer's

Gage), force the c-clamp to open against the base. The amount of force is measured by monitoring the free end deflection of the clamp with a capacitance gage (Capacitec). This deflection has been calibrated by a dead weight method and is easily converted into force. In turn, the force applied to the clamp is disturbed over the four rollers creating a load control setup. The center of the sample will experience compressive stresses toward the extrusion of the base to tensile stresses at the bottom. Knowing the load on the rollers, geometry of the sample and distance from the edge a residual stress value may be determined. Once the sample is loaded, it is optically mapped with a Sony 1394 firewire camera (Edmund Optics). This allows for locating identifiable surface features (polishing scratches or pits) that will later be used to calculate the distance from the edge of the sample. Locating the distance from the edge is done by relating the number of pixels between the edge of the sample and the feature to a calibration image, in this case a stage micrometer.

4.3.3 AFM

A Dimension 3100 atomic force microscope (AFM) with Nanoscope IV controller (VEECO Instruments, Woodbury, NY) was utilized for this experiment. A fluid cell and polymer protective skirt were employed in all testing to protect the piezoelectric scanner on the AFM. Silicon nitride (Si_3N_4) cantilevers with a reflective gold backside coating (DNP-S Veeco) and a manufacturer's spring constant of 0.58 N/m were used in the present study. The spring constant was experimentally determined prior to each study to ensure proper loading levels. Each cantilever's spring constant was determined by monitoring the deflection of the cantilever against a hard substrate (SiC) as well as a reference cantilever with known spring constant (Veeco). The cantilever and substrate act as two springs in series and the spring constant of the experimental cantilever can be deduced by equation 1 [11].

$$k_{cantilever} = \frac{(\delta_{SiC} - \delta_{RC})}{\delta_{RC}} * (k_{RC}) \qquad (1)$$

In equation 1 'δ' is the deflection and 'RC' is the reference cantilever. In addition, the radius of curvature of the probe was characterized before and after each set of experiments by a commercially available characterizer (TGT01 Micromasch, Wilsonville, OR).

4.3.4 Pseudo Physiological Solution

In order to simulate a corrosive physiological environment, phosphate buffered saline solution (PBS) (Invitrogen, Carlsbad, CA) was augmented with HCl (Fisher Scientific, Fairlawn, NJ) to a desired pH. Three values of pH were chosen to simulate the crevice environment. A pH 7.4, PBS without HCl, simulates the pH in the human body, while lower values of 5 and 3 simulate the act of differential aeration within a crevice. In addition, the pH values were chosen based on the Pourbaix diagram for chromium [12]. A pH of 7.4 is well within the thermodynamic stability region of chrome oxide, the dominant oxide covering CoCrMo [13], while a pH of 5 is right at the thermodynamic stability point and a pH of 3 is well within the thermodynamic instability region of chrome oxide.

4.4 Procedure and Data Processing

A polished specimen of CoCrMo is loaded into the c-frame where the load is measured by the capacitance gage and calibration data. A mask is placed over the frame only revealing the center cross-section of the beam between the inter-two most rollers. The sample is then optically mapped to determine identifiable features and their distance away from the edge. These features are then relocated with the camera on the AFM so that the residual stress state is predetermined before testing. Once the area is chosen 0.5-1.0mL of fluid is added to the uncovered portion forming a meniscus over the sample. The AFM scanning is performed within the bubble. A 5 μm image is taken at 2 Hz scan rate and approximately 1-2nN of force. The test is then conducted in the center of that image on an area of 2 μm x 500nm at 5 Hz (ISO 7206-7 "Endurance performance of stemmed femoral components without application of torsion" considers 5-10Hz acceptable for accelerated testing) and appropriate normal load for a duration of 15 minutes. This corresponds to the probe traveling at 10 μm/s along the fast scan axis (2 μm dimension). Under these conditions each scan line would be covered approximately 70 times along the slow scan axis (500nm dimension). After 15 minutes the scanning parameters were adjusted back to 5 μm, 2 Hz, and 1-2nN to capture the final image. Four tests of 75nN, 50nN, 25nN, and 2-3nN are conducted with a single probe in a single drop of fluid for a given surface stress state. Figure

2 depicts the experimental setup; the white boxes on the upper right inset display the testing locations. For instance, one row of white boxes indicates possible testing sites for various loadings at a given surface stress state. The probe radius of curvature is re-measured after the four tests to determine wear on the probe.

The initial and final 5μm images are used to determine the amount of material removed. Image registration is used to overlay the initial and final images. The two images are subtracted providing an indication of the volume of material removed. Average heights are taken between the unfretted areas and those in contact with the AFM probe during higher loading. The difference between these two heights gives an indication of the amount of material removed and is plotted as trench depth in the results.

It is necessary to compare trench depths based on the applied normal contact stress rather than the load since the initial probe radius of curvature will vary slightly. Hertzian contact analysis is used to determine the applied normal stress. The values for load and radius of curvature are already known from the calibration procedures. The material properties of CoCrMo and Si_3N_4 were taken as E_s= 248 GPa, E_p=310 GPa and ν_s= ν_p= 0.3 for elastic modulus and Poisson's ratio respectively [14, 15]. Where 's' denotes substrate (CoCrMo) and 'p' denotes the probe (Si_3N_4). The nominal contact pressure is determined in order to group the results.

The grouping of results by contact pressure permits four ranges to be formed: 3.6-4.0 GPa, 3.0-3.2 GPa, 2.3-2.4 GPa, and 1.0-1.3 GPa. These groups coincide with the applied loading levels of 75 nN, 50nN, 25nN, and 2-3 nN. The ranges are a result in variations of the initial tip radius and wear on the tip. As mentioned previously the radius of curvature of the tip was monitored before and after each set (4 loading levels) of experiments. The relative principal radii of curvature were found by projecting the image of the tip in two perpendicular planes and fitting a quadratic function to the data (figure 3). Figure 3 displays the quadratic fit to the projected tip images before and after the four trials. Note that the equivalent radius of curvature defined as:

$$R_e = \sqrt{R' R''} \qquad (2)$$

Where R' and R'' are the relative principal radii of curvatures determined from the graphs (fig. 3), were used in all contact analysis. In the present case the equivalent radius of

curvature varied from 40.7nm to 45.9 nm over the course of four trials. As determined from previous ambient experiments, where the tip wear could be monitored before and after each loading condition, a 3-4nm change may be attributed to the first run of 75nN followed by the remaining wear around 2nm before and after the 50nN loading trial. Insignificant wear is expected over the course of the 25nN and 2-3nN experiments. In the Hertzian contact analysis an average (before and after) equivalent radius of curvature is used to determine the contact pressure. The tip wear clarifies why the first two contact stress groups (3.6-4.0 GPa and 3.0-3.2 GPa) have a larger range than the remaining groups.

4.5 Experimental Results

Figure 4 displays the trench depth plotted against the residual stress state in the sample for each level of applied contact pressure in a pH 7.4 environment. The trench depths tend to increase as the contact pressure increases which is expected in a traditional wear situation. More interestingly is the behavior of the material due to the surface residual stress. It appears that the trench depth varies linearly with the residual stress state. The trend increases from tensile to compressive in all four contact loading conditions. When the pH is lowered with the addition of HCl this linear behavior is no longer apparent. Figure 5 displays the trench depths recorded in the pH 5.01 environment. Again the trench depths are plotted against the residual stress state and as a function of the applied contact load. The data taken at pH 5 displays a skewed quadratic trend as opposed to the linear behavior displayed at higher pH. The compressive residual stress still yields larger amounts of removed material, however; the amount of material removed from the tensile residual stress side appears to be increasing as well. This results in a skewed quadratic curve for pH of 5 and below. When the trench depth is graphed as a function of residual stress for each pH level at the highest contact stress condition the residual stress affects become more apparent (Figure 6). Only the highest contact stress for pH 3 was recorded since during the course of the experiments the tensile side experienced severe local pitting attacks. Therefore, only the initial run was deemed uncompromised being in the fluid for a little less than 20 minutes. Pitting and surface roughness evolution on the compressive side and neutral residual stress states did not appear to be as severe as the tensile side (Figure 7A and 7B).

4.6 Discussion

Previously experiments utilizing the same setup were conducted on CoCrMo in ambient conditions [16]. The trench depths were generally larger in the ambient case than those measured in the aqueous environment. This is due to the lubrication effect provided by the liquid between the probe and sample. While the applied normal contact loads would be similar, the applied shear loads at the surface are much less in the aqueous solution. If the same contact stress is compared between ambient and aqueous conditions (figure 8) it is apparent the ambient condition promotes a greater amount of wear. Interestingly though, it required around 2 GPa to elicit wear in the ambient condition whereas material is removed at around 1 GPa in the aqueous environment. This may suggest that the oxide film is somewhat unstable even at higher pH. Instability of the oxide on Stainless steel at pH 7 has been demonstrated previously [17]. When the trench depth is graphed as a function of pH (Figure 9) it becomes clear that the mechanism has changed from a purely mechanical wear phenomenon to a chemo-mechanical wear scenario.

The contact load response is similar for all mediums; a larger contact stress implies more material removal. The residual stress affects are not so straightforward between different environments. In the ambient environment as well as in pH 7.4 the trench depth varies linearly with the residual stress. This relationship may be due to a residually stressed induced delamination phenomena or an oxide repassivation phenomena or both [16]. Determining whether the repassivated oxide film may vary in composition or thickness according to the surface stress state should not be wholly discounted and is worthy of scientific exploration, however, it is outside of the scope of this paper. The role of residually stressed delamination on the other hand is much easier to argue from previous research and logical reasoning.

Work by He et al. [18] investigated the role of residual stress on crack path selection at interfaces between dissimilar elastic materials. It was determined that the residual stress plays a large role in either deflecting the crack along the interface or driving the crack into the substrate. In the case of a tensile residual stress, the propensity is for a crack to bury itself into the substrate while compressive residual stresses at the interface would promote

deflection along the interface. A finite element model created by Ye and Komvopoulos [19] examined the plastic zone size created in a ductile substrate when an indenter was actuated across a stiff film covering the substrate. In this analysis the residual stress was applied to the film itself, allowing the substrate to experience the opposite residual stress. It was determined that when the more ductile substrate was under a tensile load the plastic zones were larger, flowing into the substrate. The opposite effect was noted when the substrate was in a compressive state. The plastic zone size was reduced in the ductile substrate while the film sustained a greater amount of damage. Each study is very similar to a biomaterial system where a stiff oxide forms over a ductile substrate. These studies indicate that as damage is nucleated at the surface the ductile substrate will accept more energy dissipation if it is under a pre-tensile load while pre-compressed substrates will accept less energy dissipation. Figure 10 illustrates the hypothesized damage mechanism promoted by the AFM probe rastering across the CoCrMo interface.

Figure 11 argues strongly for a brittle fracture/delamination type of failure. Figure 11 displays four 5μm images of samples after fretting contact in pH 7.4. Figures 11A and 11B are areas under compressive loading while 11C and 11D are under approximately the same magnitude of tensile residual stress (a little over one third of the yield stress). The trenches on the compressive side are perceivable while the trenches on the tensile side are much more difficult to discern, a dashed box delineates the trench in Figure 11C. Paramount to these images is the wear debris. In Figure 11B wear debris is noted below the trench while in 11C the debris has been moved to the right of the trench. Even though a trench is difficult to perceive in 11D a small pileup of wear is detectable on the left edge. Previous experiments in the absence of fluid displayed large pileups of wear debris at the edge of the trench [16]. In the current conditions it is apparent that those large pileups were not plastic deformation of the metal substrate but rather oxide debris. The debris supports the hypothesis that the oxide film is failing by delamination/brittle failure. In figure 11A it is believed that the rastering of the AFM tip created a sufficient amount of flow to drag a majority of the particles outside of the 5 μm image although a small amount is noted along the lower 2 μm length of the trench. As mentioned previously, the delamination/brittle fracture failure is

only one part of the damage mechanism. As the pH is decreased the residually-stressed dissolution/repassivation phenomena becomes apparent.

Prior to discussing the residual-stress induced repassivation, it may be beneficial to digress and briefly discuss growth kinetics of oxide films. The thickness of an oxide film represents an equilibrium reached with the surrounding environment. As the environment changes the potential difference across the film may change giving rise to the diffusion of species thorough the film to maintain equilibrium. It is generally thought that the defects required to transport material across the film are: oxide ion vacancies, oxide ion interstitials, metal ion vacancies, and metal ion interstitials [20]. The oxide ion vacancies and metal ion interstitials will move toward the surface while metal ion vacancies and oxide ion interstitials move toward the bulk to promote film growth. Generally only the outward flux of metal ion interstitials and oxide ion vacancies are considered because the metallic cations are in general smaller than the oxygen anions. As with any chemical reaction the kinetic rate equation may be expressed as a function of the surface mobility (M) of the reaction and the driving force (F).

$$R \propto MF \qquad (3)$$

Where 'R' signifies the rate of the reaction.

Hence, it is not necessary to fully delaminate the oxide film to promote a repassivation response. As the film begins to fail by abrasive brittle fracture, diffusion of species will attempt to restore the thickness. It is possible that the residual stress in the material retards or accelerates this diffusion process. This should not dictate the entire reaction though since the residual stress is at maximum only 40% of the yield stress in the base material. It is more likely that the film is damaged, allowing the base metal to be exposed. The substrate metal is highly reactive and will undergo dissolution as well as repassivation. The local dissolution of metal into the fluid promotes the trench growth while the oxide film is not expected to recover to its full thickness. On subsequent passes of the AFM probe, this process of delamination/dissolution/repassivation will continue, slowly increasing the trench depth. As alluded to earlier previous research [7-9] has already determined that residual stress will affect the driving force (F) by altering the elastic energy density. For instance in equation 3 the driving force (F) may be defined as:

$$F = g - w - \kappa\gamma \qquad (4)$$

Where g is the free energy difference between the solid and surroundings, w is the elastic energy per unit volume, and $\kappa\gamma$ is a measure of energy related to the curvature (waviness) of the surface. Since the elastic energy density is a function of the square of the stress state the driving force will be influenced quadratically by imposed stresses; hence the repassivation/dissolution process should have a quadratic dependence on the stress state in the material, which is noted in the current experiment.

The damage mechanism by single asperity contact in terms of residual stress will proceed in the following manner. An asperity in contact with a substrate will slip causing local damage to the substrate. The amount of energy dissipated into the substrate is a linear function of the residual stress in the substrate. The oxide layer will sustain damage/delamination upon subsequent passes of the asperity. This may take the form of abrasive brittle fracture of the oxide or delamination from the metallic substrate. Diffusion of species will attempt to restore the integrity of the oxide film by repassivating (or restoring the thickness of the layer) with the surrounding environment. The residual stress will influence this process in a quadratic manner. It is interesting to note that the quadratic nature of repassivation/dissolution is only apparent at or below the thermodynamic instability point (pH) as determined from the Pourbaix diagram of chromium.

The initial damage caused by mechanically-assisted dissolution may then proceed as follows. The fretting action of local surface asperities must generate nominal contact loads in the range of 1-2 GPa to fracture/delaminate the oxide film. Fluid present in the joint may reduce these loadings acting as a hydrodynamic lubrication and preventing delamination. However, differential aeration is inevitable even if small numbers of local sites are fretted above the required loading. The subsequent decrease in the pH will lead to film instabilities. These instabilities will be enhanced at locations experiencing residual stresses either through the continuous contact loading of asperities, machining, or surface treatments. As Gilbert et al. [6] notes, the differential aeration will reach a point where the film can no longer repassivate. In our experiment this appears to be around pH 3 where localized pitting attacks alter the surface roughness to where this method is no longer applicable.

4.7 Conclusion

Asperity level fretting of CoCrMo was examined in the context of residual stresses and environment. The damage mechanism of delamination/dissolution/repassivation proposed in the mechanical-stress assisted dissolution model was investigated. It was determined that residual stress in the material enhances the delamination of the thin oxide layer in a linear manner. Compressive stress appeared to be particularly deleterious in all situations. A quadratic dependence on the stress state was noted for the dissolution/repassivation phenomena at pH below 5.

4.8 Acknowledgements

The authors would like to acknowledge helpful discussions with Dr. Sundararajan. As well as, financial support through Special Research Initiation Grant of Iowa State University.

4.9 References

[1] S. A. Brown, C. A. C. Flemming, J. S. Kawalec, H. E. Placko, and C. Vassaux, "Fretting Corrosion Accelerates crevice corrosion of modular hip tapers," *Journal of Applied Biomaterials* vol. 6, pp. 19-26, 1995.

[2] I. Catelas, J. D. Bobyn, J. B. Medley, J. J. Krygier, D. J. Zukor, and O. L. Huk, "Size, shape, and composition of wear particles from metal-metal hip simulator testing: Effects of alloy and number of loading cycles," 2003.

[3] N. J. Hallab and J. J. Jacobs, "Orthopedic implant fretting corrosion," *Corrosion Reviews*, vol. 21, pp. 183-213, 2003.

[4] N. J. Hallab, C. Messina, A. Skipor, and J. J. Jacobs, "Differences in the fretting corrosion of metal-metal and ceramic-metal modular junctions of total hip replacements," *Journal of Orthopaedic Research*, vol. 22, pp. 250-259, 2004.

[5] P. Schaff, "The role of fretting damage in total hip arthoplasty with modular design hip joints - evaluation of retrieval studies and experimental simulation methods," *Journal of Applied Biomaterials and Biomechanics*, vol. 2, 2004.

[6] J. L. Gilbert, C. A. Buckley, and J. J. Jacobs, "In vivo corrosion of modular hip prosthesis components in mixed and similar metal combinations. The effect of crevice, stress, motion, and alloy coupling," *Journal of Biomedical Materials Research*, vol. 27, pp. 1533-1544, 1993.

[7] K. S. Kim, J. A. Hurtado, and H. Tan, "Evolution of a surface-roughness spectrum caused by stress in nanometer-scale etching," *Physical Review Letters*, vol. 83, pp. 3872-3875, 1999.

[8] H. H. Yu and Z. Suo, "Stress-dependent surface reactions and implications for a stress measurement technique," *Journal of Applied Physics*, vol. 87, pp. 1211-1218, 2000.

[9] M. J. Aziz, P. C. Sabin, and G. Q. Lu, "The Activation Strain Tensor - Nonhydrostatic Stress Effects on Crystal-Growth Kinetics," *Physical Review B*, vol. 44, pp. 9812-9816, 1991.

[10] M.-W. K. Nam-Seok Park, S.C. Langford, and J.T. Dickinson, "Atomic layer wear of single-crystal calcite in aqueous solution using scanning force microscopy," *Journal of Applied Physics*, vol. 80, pp. 2680-2686, 1996.

[11] M. Tortones and M. Kirk, "Characterization of application specific probes for SPMs," *SPIE*, vol. 3009, pp. 53-60, 1997.

[12] M. Pourbaix, *Lectures on Electochemical Corrosion*. New York: Plenum Press, 1973.

[13] I. Miloslev and H. H. Strehblow, "The composition of the surface passive film formed on CoCrMo alloy in simulated physiological solution," *Electrochimica Acta*, vol. 48, pp. 2767-2774, 2003.

[14] S. P. Ho, R. W. Carpick, T. Boland, and M. LaBerge, "Nanotribology of CoCr-UHMWPE TJR prosthesis using atomic force microscopy," *Wear*, vol. 253, pp. 1145-1155, 2002.

[15] A. C. Fraker, "ASM Handbook," in *Corrosion of Metallic Implants and Prosthetic Devices*, vol. 13, pp. 1324-1335.

[16] A. Mitchell and P. Shrotriya, "Onset of nanoscale wear of metallic implant materials: Influence of surface residual stresses," Iowa State University, 2005.

[17] Z. B. N. Istephanous, J.L. Gilbert, K. Rohly, A. Belu, I. Trausch, and D. Untereker, "Oxide films on metallic biomaterials: Myths, Facts and Opportunities," *Materials Science Forum*, vol. 426-432, pp. 3157-3164, 2003.

[18] M. Y. He, A. G. Evans, and J. W. Hutchinson, "Crack Deflection at an Interface between Dissimilar Elastic-Materials - Role of Residual-Stresses," *International Journal of Solids and Structures*, vol. 31, pp. 3443-3455, 1994.

[19] N. Ye and K. Komvopoulos, "Effect of residual stress in surface layer on contact deformation of elastic-plastic layered media," *Journal of Tribology*, vol. 125, pp. 692-699, 2003.

[20] U. R. Evans, *The Corrosion and Oxidation of Metals*, 2 ed. London: Edward Arnold Ltd., 1976.

4.10 Figure Captions

Fig. 1 Bird's eye view of frame as well as an isometric view (right). The major components of the bending frame consist of a c-clamp, base, capacitance gage, rollers, and sample.

Fig. 2 Illustration of the experimental setup. The upper right inset depicts the possible locations of testing sites (white boxes). The lower left inset illustrates a probe rastering across one particular testing site demonstrating the wear debris formation and chemical dissolution taking place.

Fig. 3 Figure 3 portrays four images of the probe. The top two images are profiles and curves fits to the projection of the probe before the testing was started. The lower two images display the two relative principal radii of the curvature after four trials at 75nN, 50nN, 25nN, and 2-3nN.

Fig. 4 Results from the pH 7.4 solution. The trench depth is plotted against the normalized residual stress. The yield strength of the material (450 MPa) is used as a normalization value. Error bars are excluded for clarity.

Fig. 5 Results from the pH 5.01 solution. The trench depth is plotted against the normalized residual stress. The yield strength of the material (450 MPa) is used as a normalization value.

Fig. 6 Results of the highest contact loading condition for each solution.

Fig. 7 Pits formed on the surface as a result of low pH. A) CCD image of the compressive side of the beam after being exposed to PBS+HCl for a little over 1 hour. B) Tensile side of the beam after the same test. C) and D) Corresponding images to A and B respectively. The scale bar in the left corner is 50 μm. The background "noise" (flat surface) is subtracted out to highlight the pitted areas in C and D.

Fig. 8 Plot of the ambient data obtained previously against the highest contact loading level in the pH 7.4 environment. The contact stress is similar in each condition.

Fig. 9 Trench depth plotted for the highest contact loading condition at three residual stress states as a function of pH.

Fig. 10 Illustration of the hypothesized damage mechanism occurring as the AFM probe actuates across the surface. The upper right inset display the metal dissolution caused by the lower pH as well as the competitive process of repassivation.

Fig. 11 A) Final 5 μm AFM scan of the fretted area after 75nN (3.6-4.0 GPa) contact loading for 15 minutes in a solution of pH 7.4 and a compressive residual stress level of approximately one-third of the yield stress. B) 25nN (2.3-2.4 GPa) contact loading at the same compressive residual stress state. C) 5 μm AFM scan of the wear scar (white boxed area) produced after 75 nN of loading on a tensile residual stressed portion equivalent to about one third of the yield stress. D) Final 5 μm AFM scan after 25nN of contact load on an equivalent tensile stress as C.

Fig. 1

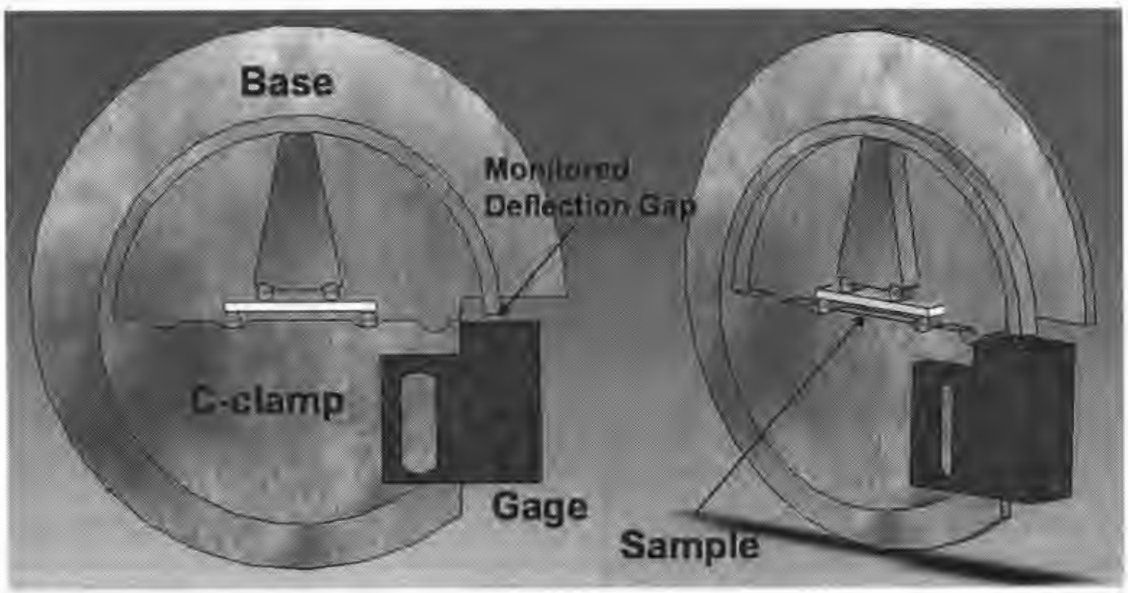

Fig. 2

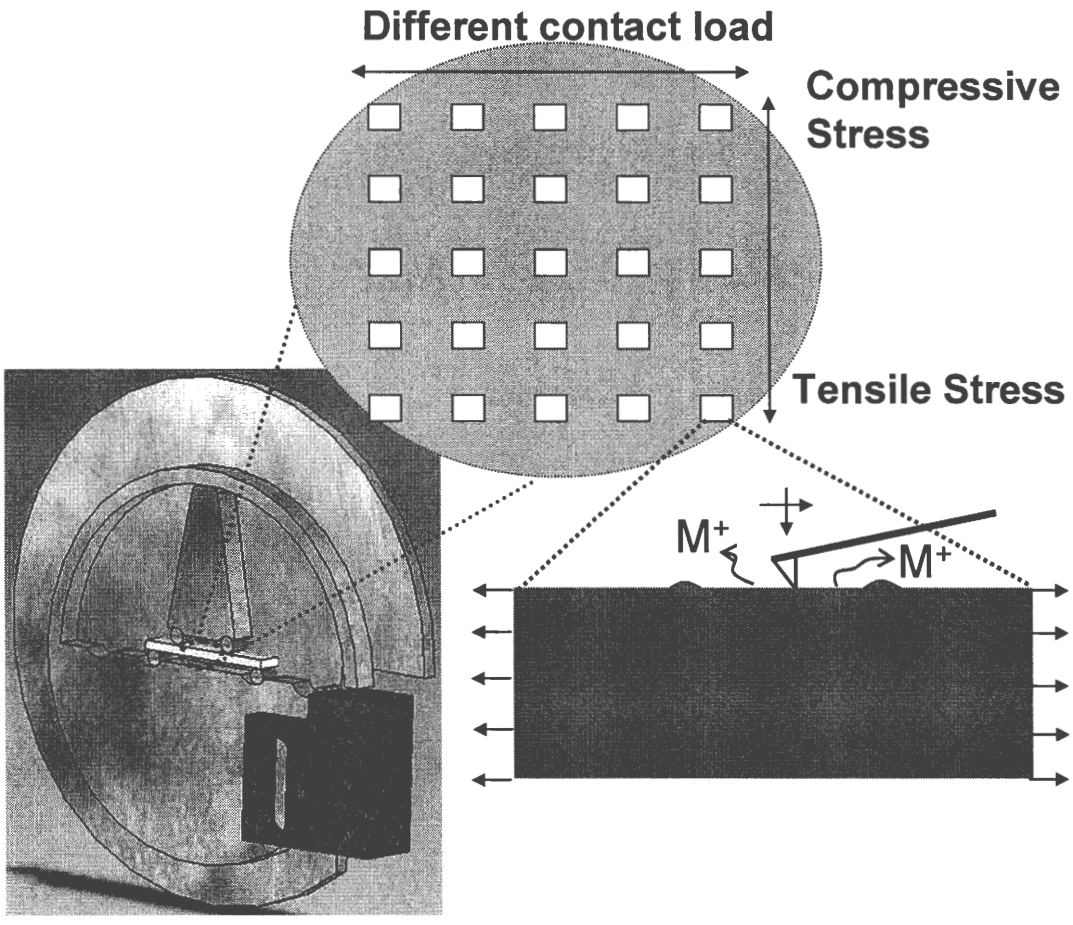

Fig. 3

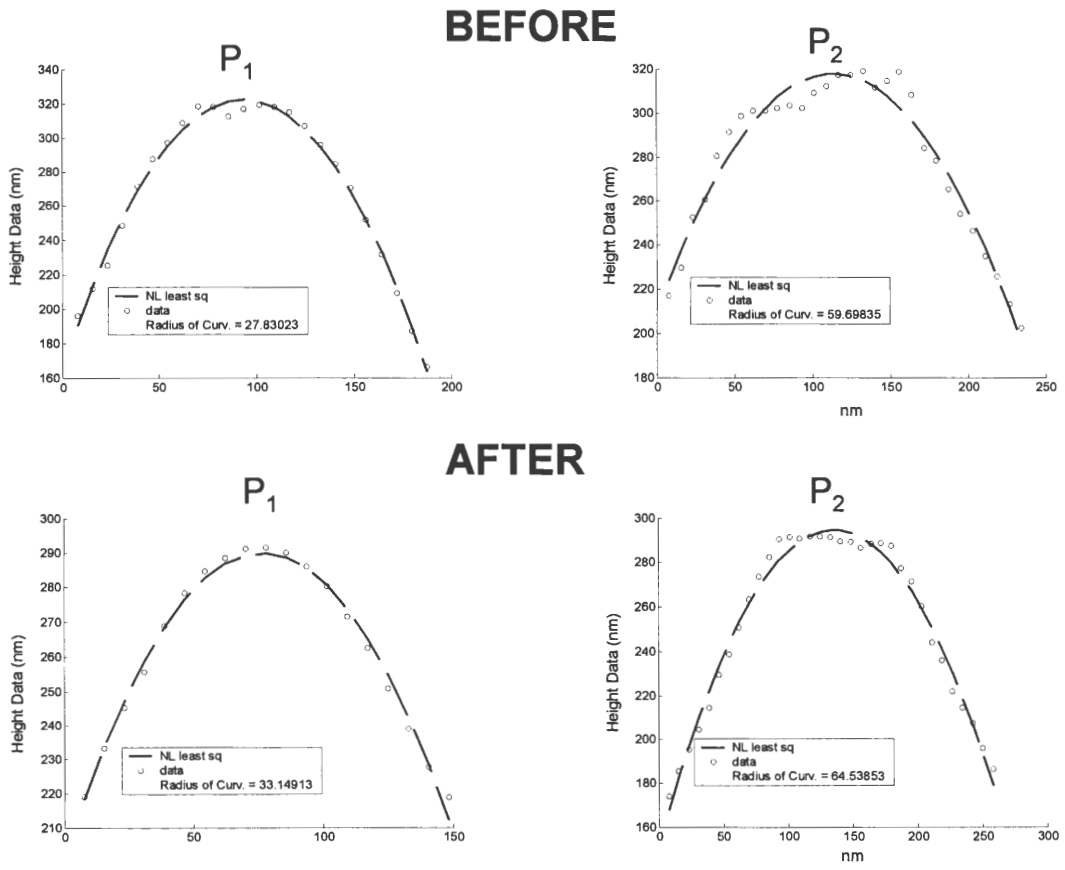

Fig 4

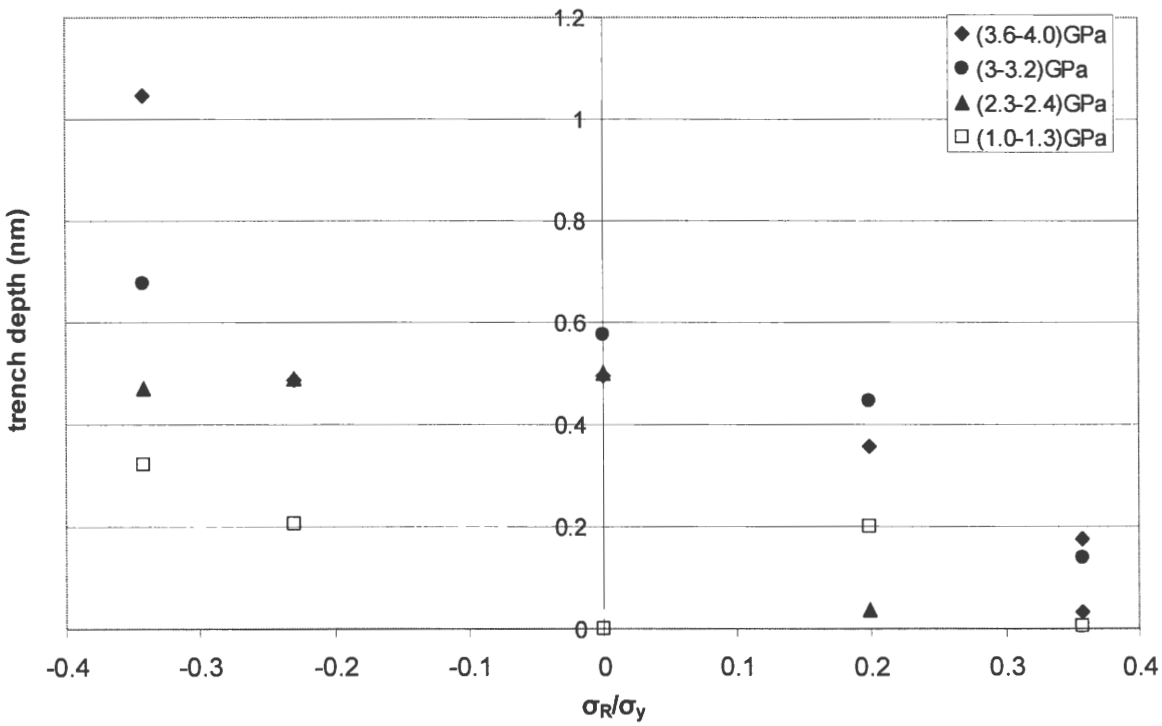

Fig. 5

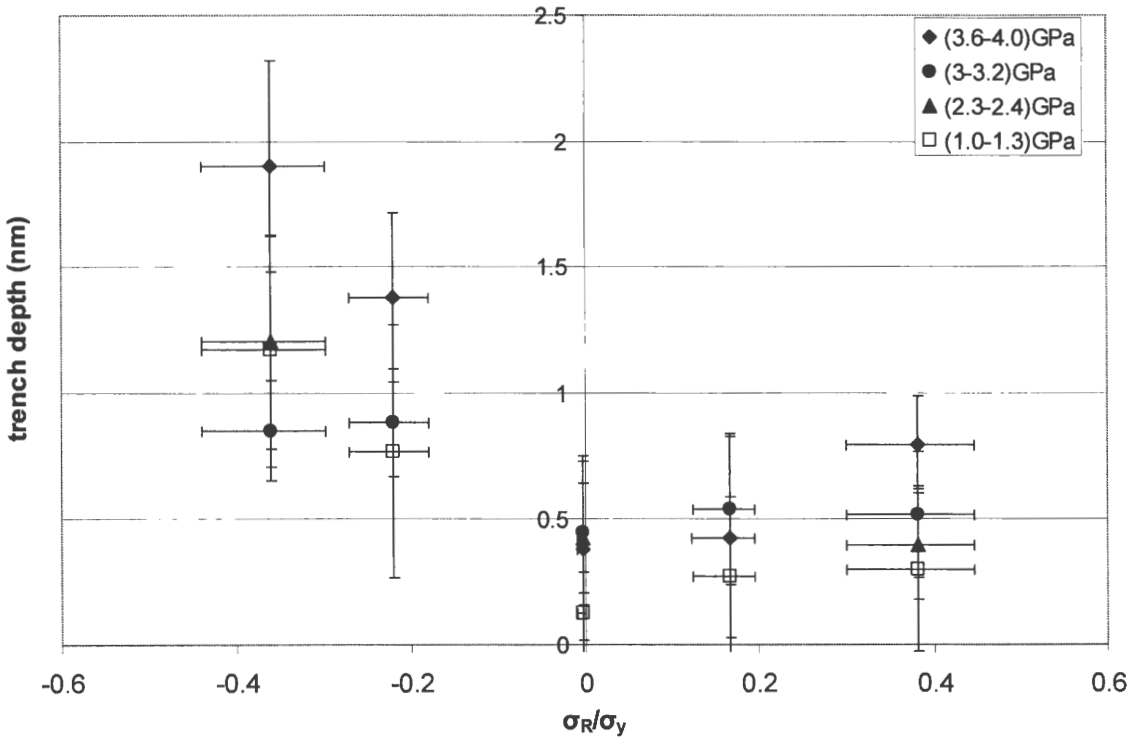

Fig. 6

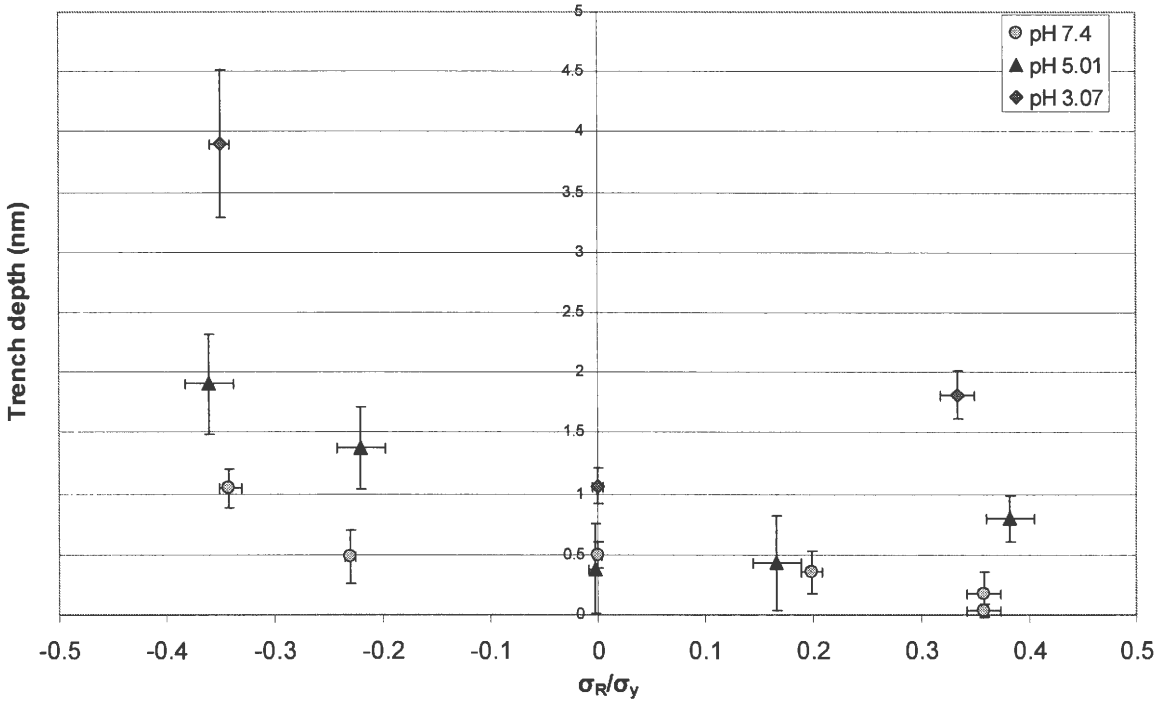

Fig. 7

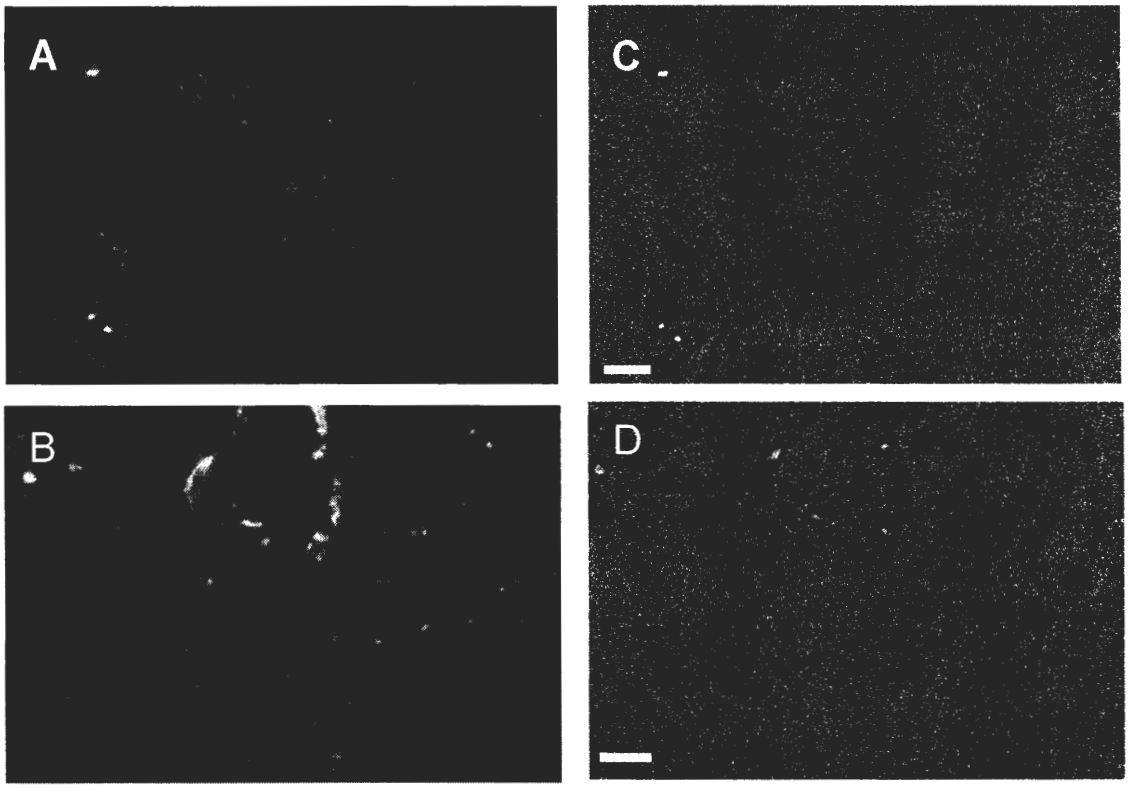

Fig. 8

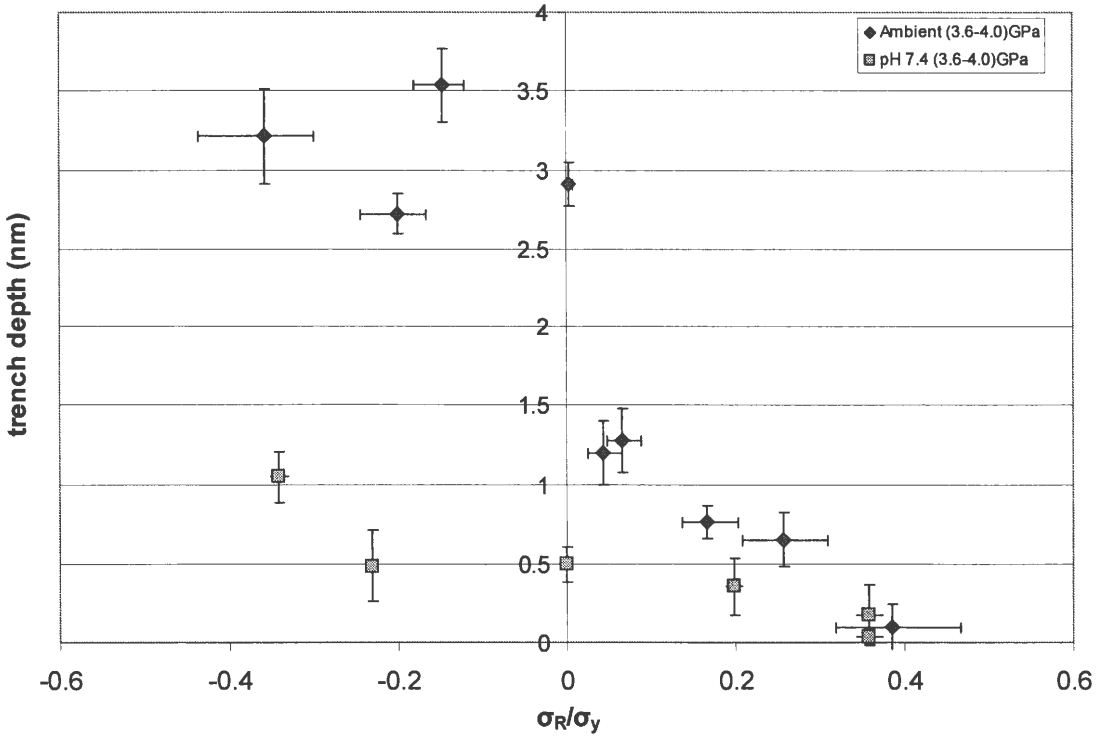

Fig. 9

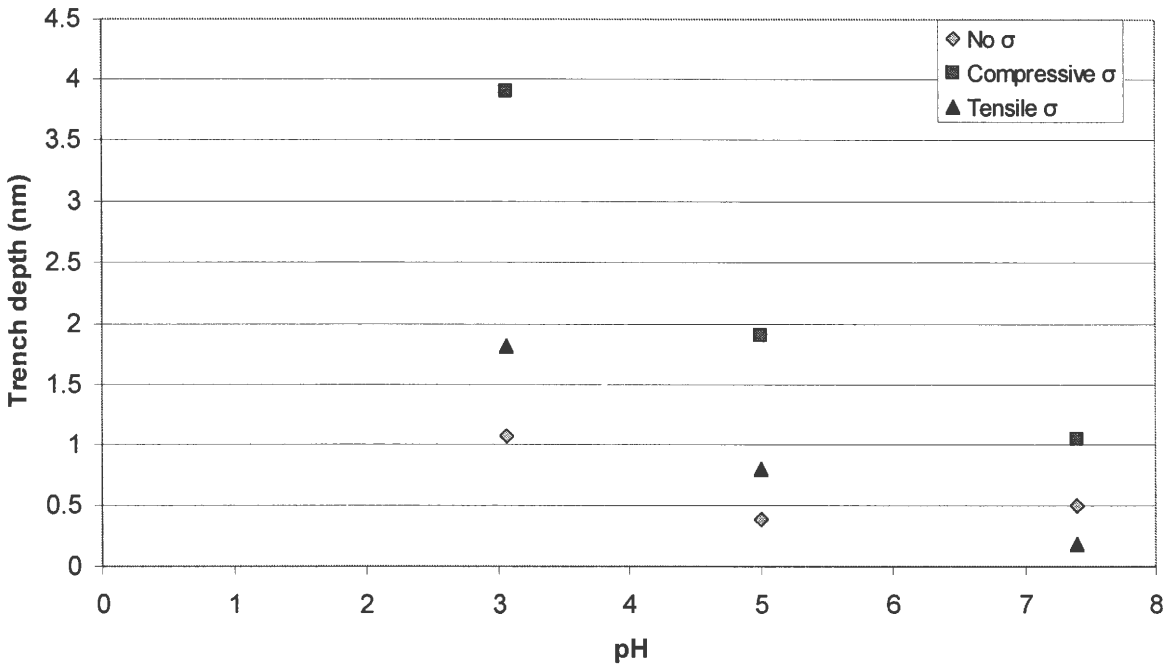

Fig. 10

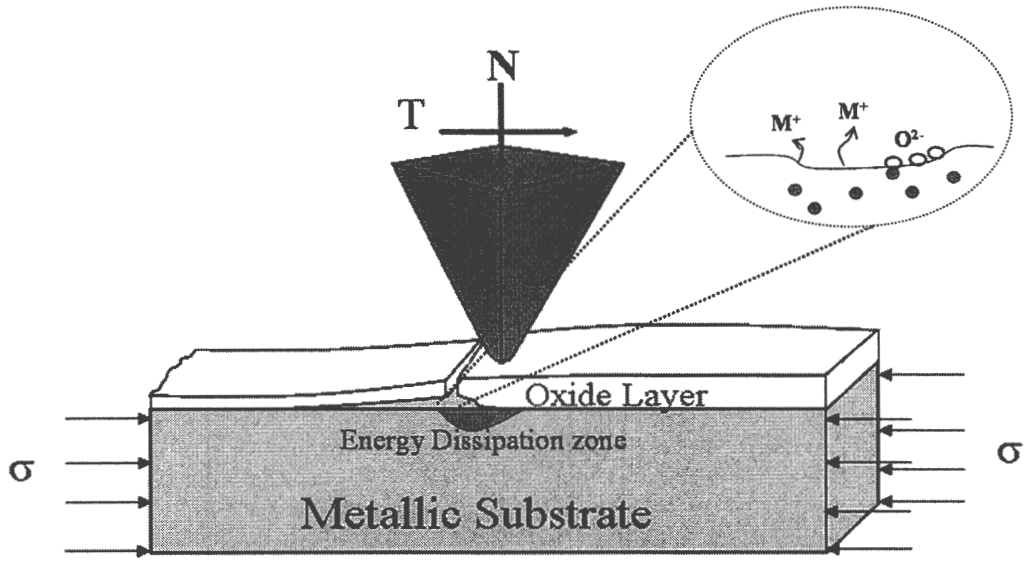

Fig. 11

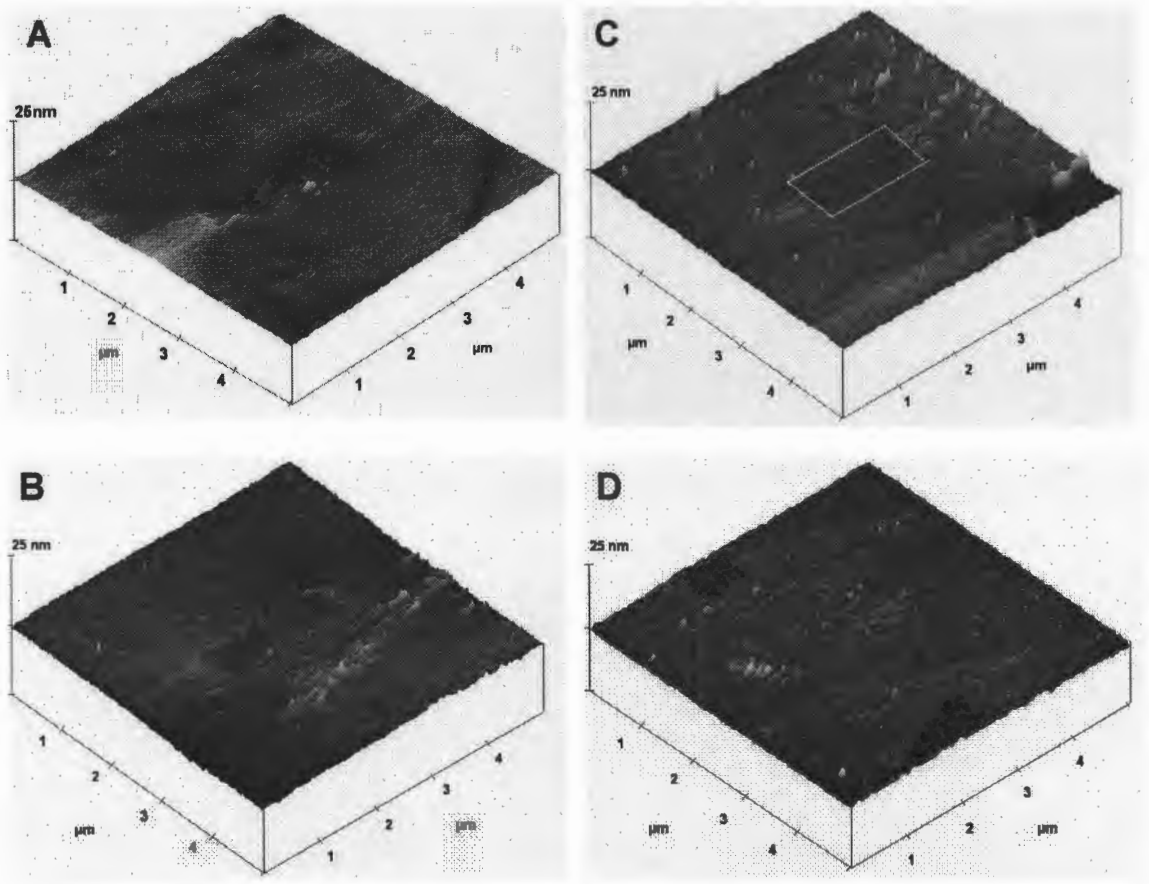
A
25nm
1
2
3
4
µm
1
2
3
4
µm
C
25 nm
1
2
3
4
µm
1
2
3
4
µm
B
25 nm
1
2
3
4
µm
1
2
3
4
µm
D
25 nm
1
2
3
4
µm
1
2
3
4
µm

Chapter 5. Conclusions

5.1 General Conclusions

The surface failure of CoCrMo was examined in the context of residual stress, contact loading, and environment. A novel experimental technique incorporating a four point bending frame in conjunction with an atomic force microscope provided a first glimpse at the effects of residual stress on nanoscale deformation. This technique allows for known levels of surface residually stressed material to be probed/scratched with well-characterized contact loads with nanoscale resolution.

In order to simulate a residual stress in the material a four point bending frame was designed to be used in conjunction with an atomic force microscope. The frame supplies residual stress levels varying from compressive to tensile across the sample. The characterization of the stress state only requires knowledge of the distance from the neutral axis. Coupling this technique with the unparalleled resolution of the AFM provides the unique opportunity to study residual stress induced failure on the nanoscale.

In the ambient environment a linear trend was noted between the residual stress and trench depths created. Compressive residual stresses facilitated the deformation of the CoCrMo alloy while tensile stress mitigated the damage. Higher contact loads elicit larger trench depths while the minimum nominal contact stress required to initiate deformation must be greater than 2.5 GPa for any residual stress state for the given number of loading cycles. Utilizing previous work from thin film and fracture mechanics models, a hypothesis was set forth relating the surface damage to residual stress in the ductile substrate. The aqueous environment displayed a slightly different behavior.

In the aqueous environment the trench depth was linearly dependent on the residual stress state for stable pH (7.4). As the pH approached the thermodynamic instability point (pH 5 from the Pourbaix diagram for Chromium) the trench depth (wear) began to appear as a quadratic function of the residual stress. This skewed quadratic nature is a superposition of the linear relationship imposed by the energy dissipation into the substrate and the quadratic behavior of the dissolution/repassivation imposed by the increase in strain energy term in the driving force relation.

5.2 Significant Findings

To the authors knowledge these studies are the first to experimentally demonstrate the effects of a controlled residual stress field on the damage imposed by an asperity level contact. Furthermore, this study is the first to introduce:

- A linear deformation mechanism imposed by the residual stress state for metals with naturally occurring oxides in ambient conditions.
- A quadratic relationship between the dissolution/repassivation mechanism and the residual stress state when the oxide layer is destabilized by repeated contact loading.

5.3 Future Work

It is the hope of the author that the experimental results will lead to a comprehensive damage model incorporating the mechanical stimulation and material kinetics. At the current time a model is being discussed but has not reached fruition. In addition to the current results, experiments incorporating other materials may be desirable. Presently, experiments with copper alloys are being investigated. Copper results will provide complementary information regarding the damage mechanisms. For instance, copper is noble and will resist corrosion as opposed to the anodic base material Chromium. Also, the mechanical damage mechanism is expected to change since Cu-alloys do not form as tenacious of an oxide layer as CoCrMo alloys.